Check for updates

Earth's Future

RESEARCH ARTICLE
10.1029/2022EF002776

Contrasting Fate of Western Third Pole's Water Resources Under 21st Century Climate Change

Fengge Su[1], Hamish D. Pritchard[2], Tandong Yao[1], Jingheng Huang[1], Tinghai Ou[3], Fanchong Meng[1,4], He Sun[1], Ying Li[1,5], Baiqing Xu[1], Meilin Zhu[1], and Deliang Chen[3]

[1]State Key Laboratory of Tibetan Plateau Earth System, Resources and Environment, Institute of Tibetan Plateau Research, Chinese Academy of Sciences, Beijing, China, [2]British Antarctic Survey, Cambridge, UK, [3]Regional Climate Group, Department of Earth Sciences, University of Gothenburg, Gothenburg, Sweden, [4]College of Geosciences and Engineering, North China University of Water Resources and Electric Power, Zhengzhou, China, [5]College of Hydraulic & Environmental Engineering, China Three Gorges University, Yichang, China

Key Points:

- Contrasting patterns of water future are observed across four major mountain basins in the western Third Pole dictated by hydroclimatic regimes
- Glacier meltwater will continuously contribute to the increasing summer and annual water supplies in the upper Indus and Yarkant
- Syr Darya will face enhanced summer water shortage and increased wet and dry hydrological extremes due to shifted meltwater fluxes

Supporting Information:

Supporting Information may be found in the online version of this article.

Correspondence to:

F. Su,
fgsu@itpcas.ac.cn

Citation:

Su, F., Pritchard, H. D., Yao, T., Huang, J., Ou, T., Meng, F., et al. (2022). Contrasting fate of western Third Pole's water resources under 21st century climate change. *Earth's Future*, *10*, e2022EF002776. https://doi.org/10.1029/2022EF002776

Received 16 MAR 2022
Accepted 8 SEP 2022

Author Contributions:

Conceptualization: Fengge Su, Hamish D. Pritchard, Tandong Yao
Data curation: He Sun, Baiqing Xu, Meilin Zhu
Formal analysis: Fengge Su, Jingheng Huang, Tinghai Ou, Fanchong Meng, He Sun
Investigation: Fengge Su, Jingheng Huang, Fanchong Meng, Baiqing Xu, Meilin Zhu

© 2022 The Authors. Earth's Future published by Wiley Periodicals LLC on behalf of American Geophysical Union. This is an open access article under the terms of the Creative Commons Attribution-NonCommercial-NoDerivs License, which permits use and distribution in any medium, provided the original work is properly cited, the use is non-commercial and no modifications or adaptations are made.

Abstract Seasonal melting of glaciers and snow from the western Third Pole (TP) plays important role in sustaining water supplies downstream. However, the future water availability of the region, and even today's runoff regime, are both hotly debated and inadequately quantified. Here, we characterize the contemporary flow regimes and systematically assess the future evolution of total water availability, seasonal shifts, and dry and wet discharge extremes in four most meltwater-dominated basins in the western TP, by using a process-based, well-established glacier-hydrology model, well-constrained historical reference climate data, and the ensemble of 22 global climate models with an advanced statistical downscaling and bias correction technique. We show that these basins face sharply diverging water futures under 21st century climate change. In RCP scenarios 4.5 and 8.5, increased precipitation and glacier runoff in the Upper Indus and Yarkant basins more than compensate for decreased winter snow accumulation, boosting annual and summer water availability through the end of the century. In contrast, the Amu and Syr Darya basins will become more reliant on rainfall runoff as glacier ice and seasonal snow decline. Syr Darya summer river-flows, already low, will fall by 16%–30% by end-of-century, and striking increases in peak flood discharge (by >60%), drought duration (by >1 month) and drought intensity (by factor 4.6) will compound the considerable water-sharing challenges on this major transboundary river.

Plain Language Summary The western Third Pole (TP) is the most glacierized (>50% of the region) and snow-concentrated areas in the region. Climate-driven changes to the cryosphere in upper mountains in the TP have raised a major concern on the downstream water supply. However, the runoff regime and future water availability of the region are inadequately quantified. Here, we systematically assess the future evolution of runoff in total water availability, seasonal shifts, and dry and wet discharge extremes in four most meltwater-dominated basins in the western TP by using a process-based glacier-hydrology model, well-constrained historical and future climate data. We show that these basins face sharply diverging water futures under 21st century climate change. In the upper Indus and Yarkant, enhanced glacier melt will continue acting as a major water source in summer and annual water supply by the end of this century, especially under the highest emission scenario, but considerably increasing the extreme floods in the Indus. In contrast, the Syr Darya will face a declining annual water supply and increasing extreme spring floods and summer water shortages, as its glaciers retreat and snowmelt arrives earlier in the spring, further complicating the water resource management in this transboundary river.

1. Introduction

The Tibetan Plateau and adjacent mountains, also known as the Third Pole (TP), contain extensive snow coverage (~19%) (Barnett et al., 2005; Li et al., 2018) and the largest number of glaciers outside the Polar Regions (97,605 km^2) (RGI Consortium, 2017). Glaciers in the TP have strongly responded to recent climate change (Bhattacharya et al., 2021; Bolch et al., 2012; Yao et al., 2012) and are projected to continue to retreat through the 21st century (Huss & Hock, 2018; Kraaijenbrink et al., 2017; Rounce, Hock, & Shean, 2020), raising a major concern on downstream water supply for agriculture, ecosystems, hydropower, and human society (Biemans et al., 2019; Kaser et al., 2010; Milner et al., 2017; Pritchard, 2019).

Methodology: Fengge Su, Tinghai Ou
Software: Jingheng Huang, Tinghai Ou, Ying Li
Validation: Jingheng Huang, Fanchong Meng, He Sun, Baiqing Xu
Visualization: Tandong Yao, Tinghai Ou, Ying Li, Deliang Chen
Writing – original draft: Fengge Su, Hamish D. Pritchard
Writing – review & editing: Hamish D. Pritchard, Deliang Chen

However, glacier melt is not critically important to water supply everywhere in the TP, with a negligible or moderate contribution to annual runoff in the southeastern monsoon basins with relatively limited glacier coverage (e.g., the upper Yellow and Mekong) (Lutz et al., 2014; Zhang et al., 2013; Zhao et al., 2019). The most glacierized (>50% of the region) and snow-concentrated areas lie in the western TP (Figure 1), among the Tian Shan, Pamir, Karakoram, Hindu-Kush, and western Himalayan Mountain ranges, where the climate is mainly controlled by the midlatitude westerlies with winter and spring snowfall frequently dominating annual precipitation totals (Cannon et al., 2016; Maussion et al., 2014). Melt water from glaciers and seasonal snow is of particular importance to ecosystems and human society in the downstream river basins with relatively hot, dry summers and periodic droughts (Biemans et al., 2019; Kaser et al., 2010; Milner et al., 2017; Pritchard, 2019). The western TP basins of Syr Darya and Arm Darya in the Aral Sea basin, Tarim, and Indus (Figure 1) belong to this category, with their lowlands heavily relying on mountain water resources (Chen et al., 2018; Duethmann et al., 2015; Immerzeel & Bierkens, 2012; Immerzeel et al., 2010; Kan et al., 2018; Nezlin et al., 2004). The mountain catchments of these basins have been identified as the most important and highly vulnerable Asian "water tower units" in terms of their water supply and downstream water demands, combined with conflicting seasonal demands on their water resources among upstream and downstream nations (De Stefano et al., 2017; Immerzeel et al., 2020; Sorg et al., 2014; Varis & Kummu, 2012).

The future water availability of the region, and even today's runoff regime, however, are both hotly debated and inadequately quantified. Challenges primarily stem from a lack of representative meteorological information in high elevations (Dahri et al., 2016; Immerzeel et al., 2015; Kan et al., 2018; Pritchard, 2021; Unger-Shayesteh et al., 2013; Wortmann et al., 2018), inadequate representation of glacier-hydrological process, and large spreads in future climate projections and downscaling approaches (Kraaijenbrink et al., 2017; Su et al., 2013), hindering a comprehensive understanding on the flow regime and future water availability in the mountainous TP (Pellicciotti et al., 2012; Ragettli et al., 2013, 2016). Precipitation regimes are poorly represented by in situ observations or multi-sensor-based gridded datasets across the TP region (Dahri et al., 2016; Immerzeel et al., 2015; Kan et al., 2018; Palazzi et al., 2013; Sun & Su, 2020; Sun, Su, He, et al., 2021; Tong et al., 2014; Wortmann et al., 2018) due to complex terrain, heterogeneous station networks, and diverse climate conditions across the region, and gridded products usually need correction before they can be used for hydrological modeling (Dahri et al., 2021; Li et al., 2020; Sun, Su, He, et al., 2021, Sun, Su, Yao, et al., 2021; Tong et al., 2014; Wortmann et al., 2018). Recent modeling studies over the TP tend to either directly use the grid data (e.g., reanalysis precipitation) as model input (e.g., Khanal et al., 2021; Kraaijenbrink et al., 2017, 2021) or treat the reanalysis precipitation or temperature as calibrated parameters to match glacier mass balance observations (Rounce, Hock, & Shean, 2020; Rounce, Khurana, et al., 2020). However, the known uncertainties in the reanalysis precipitation leave the modeling results or real precipitation distribution in the study regions highly uncertain.

Distributed cryospheric-hydrological models, properly validated with recorded data, are currently one of the most feasible approaches to characterize runoff regime and their responses to climate changes. Climate impact studies have been conducted in the upper Indus with different complexity of hydrological models (Biemans et al., 2019; Immerzeel et al., 2010; Khanal et al., 2021; Lutz et al., 2014, 2016; Su et al., 2016; Wijngaard et al., 2017; Zhang et al., 2013), however variations in input data, modeling approach and choice of future climate scenario have produced divergent and even contradictive results (Table S1 in Supporting Information S1), making the future water availability in the upper Indus highly uncertain. On the other hand, quantitative studies on the interaction of glacier, hydrology and climate change are quite limited in the Aral Sea and Tarim basins (Duethmann et al., 2015, 2016; Luo et al., 2018; Wortmann et al., 2022; Zhao et al., 2015). Studies either mostly focused on the highly glacierized upper branches of the Syr Darya or Amu Darya (Gan et al., 2015; Hagg et al., 2013; Sorg et al., 2014), or at regional scale explorations with conceptual approaches (Alford et al., 2015; Immerzeel & Bierkens, 2012; Siegfried et al., 2011). Moreover, regional or global scale assessments (e.g., Huss & Hock, 2018; Pritchard, 2019; Rounce, Hock, & Shean, 2020; Rounce, Khurana, et al., 2020) tend to only consider water yields from glaciers, with runoff processes in non-glacierized areas either omitted or greatly simplified.

Under the ongoing and expected continued atmospheric warming in the centuries ahead (IPCC, 2014), characters of runoff are expected to alter in both mean flow regimes and the magnitude and timing of flow extremes due to changes in the runoff sources of rain, snow and glacier melt (e.g., Blöschl, et al., 2017; Braun et al., 2000; Horton et al., 2006; Khanal et al., 2021; Middelkoop et al., 2001; Siegfried et al., 2011), potentially exacerbating downstream seasonal water stress and the risk of natural hazards (i.e., climate-change-induced floods and droughts). Hydrological projection studies in the TP so far have mainly focused on the impacts of future climate change on total water availability and seasonal changes (Khanal et al., 2021; Lutz et al., 2014; Su et al., 2016; Zhao

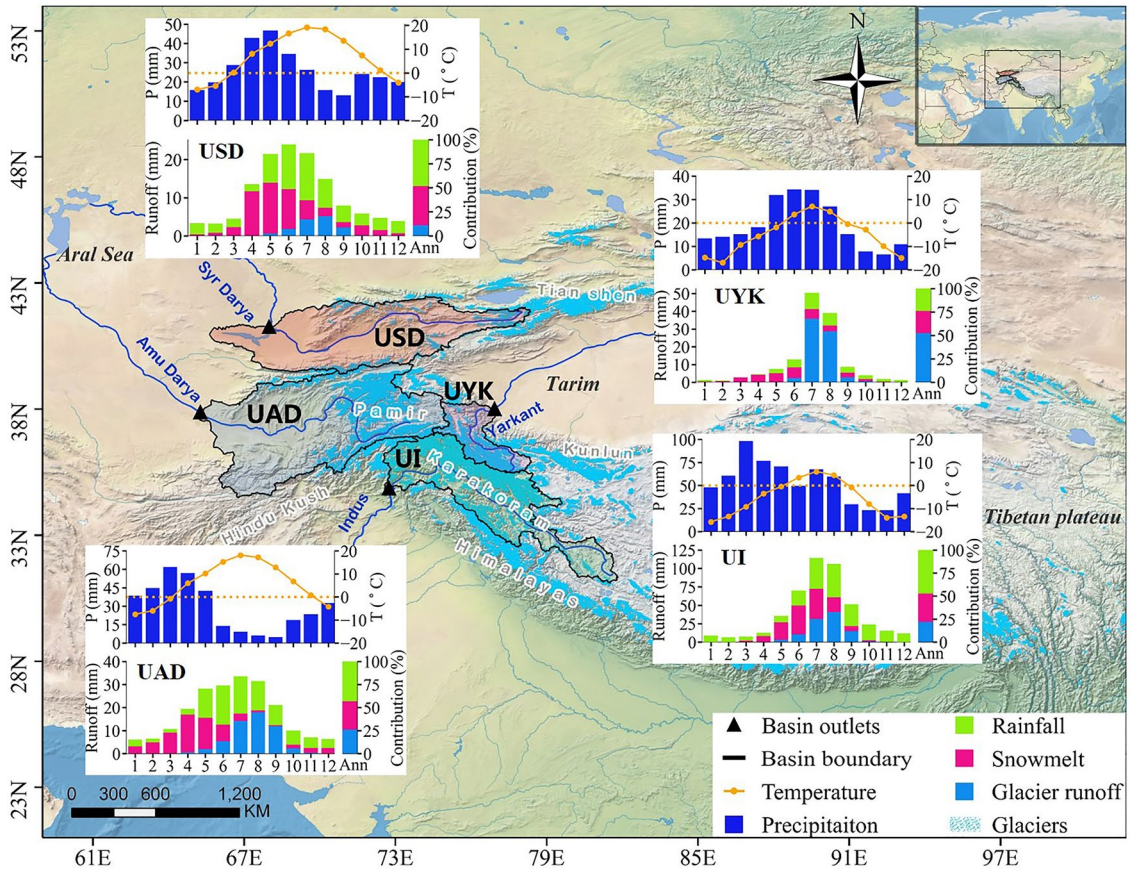

Figure 1. The upper basins of Syr Darya, Amu Darya, Yarkant and Indus (UI). Bar and dotted-line plots show the seasonal distribution of basin-averaged precipitation, temperature, and simulated runoff components (rainfall runoff, snowmelt runoff, and glacier runoff), and the contribution of each to annual total flow (%) at the basin outlets (black triangle) in the reference period of 1971–2000 (1980–2000 for the UI).

et al., 2019); few studies have been conducted on the future hydrological extremes changes which are highly relevant to human life and substantial socioeconomic and environmental damages, especially in densely populated and/or ecologically vulnerable areas (Dahri et al., 2021; Hoang et al., 2016; Sauer et al., 2021; Shukla & Sen, 2021). Among the limited studies, Lutz et al. (2016) and Wijngaard et al. (2017) had a focus on the upper Indus, Ganges and Brahmaputra basins, while the relevant studies are still lacking in the Aral Sea and Tarim basins.

Here, we close this knowledge gap by systematically assessing future changes in annual, seasonal, and extreme high and low river flows in four western TP basins, including the upper Syr Darya (USD) and Amu Darya (UAD), upper Yarkant (UYK) in the Tarim basin, and upper Indus (UI) (Figure 1; Table 1). The unique features of these four basins as mentioned early (the most snow- and glaciers-concentrated regions in the western TP, high dependence of their dry lowlands on the mountain water resources, and being identified as most important and vulnerable Asian water tower units) highlight the needs for comprehensive assessments on the future river flow changes at different time scales for water management, decision makers, climate change adaptation and hazards mitigation in these complex transboundary river basins. To this end, we first quantify the flow regimes of the four upper basins under the present climate with a process-based, well-established glacier-hydrology model (VIC-glacier) and well-controlled historical reference climate data. Subsequently, we investigate the evolution of annual-average and seasonal-average river discharge and the wet and dry extremes for these four basins through the 21st century, using global climate models (GCM) projections under Representative Concentration Pathway (RCP) 4.5 (with emissions peaking around 2040–2050 then declining), and RCP8.5 (emissions rising throughout the 21st century). The representation of future hydrology is highly dependent on the selection of GCMs which are used to force the hydrological models (Khanal et al., 2021; Lutz et al., 2014, 2016; Wijngaard et al., 2017). Multi-model ensemble mean generally shows better agreement with observations than does any single model (Li et al., 2021; Su et al., 2013). Here, the ensemble of monthly precipitation and temperature projections from 22 GCMs (Table S7 in

Table 1
Characteristic of the Four Upper Western Basins in the Third Pole

Basin	UYK (Tarim)	UI	USD	UAD
Control station	Kaqun	Besham	Chardara	Kerki
Latitude (°N)	37.98	34.92	41.24	37.83
Longitude (°E)	76.9	72.88	67.97	65.25
Drainage area (km^2)	46,704	162,896	200,300	284,800
Elevation (m)	1450	4323	1769	2532
[a]Glacier coverage (%)	9.3	11.9	0.9	3.4
Glacier area (km^2)	4,343 (18,569)	19,385	1,803	9,683
[b]Mean annual now cover Fraction (%)	33.7	35.6	33.0	37.0

[a]Glacier data from the Randolph Glacier Inventory V6.0, http://www.glims.org/RGI/. [b]Snow cover fraction data from the Moderate Resolution Imaging Spectroradiometer (MODIS)10C2, https://nsidc.org/data.

Supporting Information S1) are statistically bias-corrected and downscaled to gridded daily transient climate forcing of 2006–2099, which allow the evolution of meltwater contribution and hydrological extremes to be assessed over the study basins. This work is first to systematically assess the transient flow evolution at annual, seasonal, and daily (both wet and dry discharge extremes) scales from present to the end of 21st century in the four western TP basins. The following novel components are expected to advance our understanding of present and future hydrological process in these most meltwater-impacted basins in the TP: (a) well-controlled and validated reference climate data; (b) well-developed and -validated hydrological model which includes all relevant cold processes; (c) a wide range of future climate scenarios (22 GCMs × 2 RCPs) with an advanced statistical downscaling technique.

2. Study Area

The UYK, UI, UAD, and USD are defined as all regions upstream of the Kaqun, Besham, Chardara, and Kerki hydrological stations, respectively (Figure 1 and Table 1). The UYK, originating from the north Karakoram ranges, is a major tributary of the Tarim basin providing water to the fourth largest irrigation system in China (Chen et al., 2007). The USD and UAD (Figure 1), originating from the Tien Shan and Pamir mountains, respectively, provide the major water supply for downstream of the Aral Sea basin. Moreover, the Syr Darya and Amu Darya are two of the most complex transboundary rivers in the world, with conflicts of international water allocation since the collapse of the Soviet Union (Bernauer & Siegfried, 2012). The UI, originating from the Hindukush-Karakoram-Himalaya (HKH) mountain ranges (Figure 1), supplies the largest continuous irrigation system in Asia and sustains livelihoods of millions of people downstream (Immerzeel & Bierkens, 2012; Immerzeel et al., 2010).

The climate, particularly precipitation, of the study areas is generally modulated by the midlatitude westerlies with 50%–70% of annual precipitation occurring in November-April in the UI, UAD, and USD (Figure 1); however, precipitation regime varies among the four basins. In the UYK, more than 60% of annual precipitation occurs during May–September due to the orographic barrier created by the Pamir-Tian Shan mountains, which restricts the moisture from the westerlies (Baldwin & Vecchi, 2016; Wang et al., 2020). The UI is affected by both the winter westerlies and the Indian summer monsoon (Palazzi et al., 2013), with about 32% of annual precipitation in June-September (Table S5 in Supporting Information S1). Glacier distribution is highly uneven among the four basins, with the least glacier coverage of 0.9% in the USD and the largest ice area in the UI and UYK (11.9% and 9.3%, respectively) (Table 1). Snow distribution is relatively uniform, with the mean annual snow cover fraction (SCF) of 33%–37% among the four basins. The variations in the precipitation regime and glacier distribution highly determine the runoff response to future climate changes in the study basins.

3. Data and Methods

3.1. Data

3.1.1. Historical Climate Data

Given the varying basin size (from 46,704 to 284,800 km^2, Table 1), diverse climate, surface characters, and station conditions, no single correction approach can fit all basins (Dahri et al., 2016, 2018; Immerzeel

et al., 2015; Kan et al., 2018; Sun & Su, 2020; Wortmann et al., 2018). In this work, we used daily gridded precipitation and temperature data at 10×10 km grids from recently generated and well constrained gridded data (Huang et al., 2022; Kan et al., 2018), involving corrections using gauge measurements or reanalysis data, in the UYK, USD and UAD for 1961–2015, and the UI for 1980–2015. In the UYK (Kan et al., 2018), the daily gridded precipitation and temperature data were generated based on precipitation and temperature gradient observations and automatic weather stations (AWS) at high elevations, and meteorological stations at low elevations (Figure S1a in Supporting Information S1). In the USD and UAD (Huang et al., 2022), the gridded climate input data were generated through corrections of the Princeton Global Meteorological Forcing Data set for land surface modeling data (PGMFD) reanalysis data (Sheffield et al., 2006) based on 122 selected precipitation gauges by combining orographic and linear correction approaches (Huang et al., 2022; Sun & Su, 2020). In the UI, the daily gridded precipitation for 1980–2015 were generated through corrections of the reanalysis data of MERRA-2 (Gelaro et al., 2017; Reichle et al., 2017), with an inverse modeling approach. Observed runoff, glacier area and glacier mass changes from literature (Table S4 in Supporting Information S1) were used as multiple criteria for the correction of MERRA-2 at mean annual scales. More details on the climate data generation and validation for each basin can be found in Text S1 in Supporting Information S1. The generated climate data was extensively validated through: (a) comparing independent precipitation gauges with the corresponding grids (Figures S1–S3 in Supporting Information S1), and (b) inverse hydrological modeling against the discharge, snow cover fraction, and glacier area/mass change observations in the study basins (Figures S4–S8 in Supporting Information S1). The well constrained historical precipitation data largely contributes to reducing uncertainties in the calibrated model parameters and hydrological simulations and predictions.

3.1.2. Other Data

A list of other data for the VIC-glacier model setup and calibration and validation are summarized in Table S3 in Supporting Information S1, including the digital elevation model (DEM), land use, soil texture, streamflow, glacier, and snow data.

3.2. Methods

3.2.1. Glacier-Hydrology Model

In this work, we use the Variable Infiltration Capacity (VIC) (Liang et al., 1994, 1996) large-scale land surface hydrological model coupled with a degree-day glacier melt algorithm (Hock, 2003; Zhang et al., 2013; Zhao et al., 2015). This improvement allows us to simulate the hydrological processes in large-scale mountainous basins with glaciers. VIC is a physically based, distributed hydrological model that parameterizes the water and energy exchanges among soil, vegetation, and atmosphere over a grid mesh. The VIC model is characterized by the representation of multiple land cover types, spatial variability of soil moisture capacity, soil water flows between three soil layers, surface flow considering the heterogeneity of saturation excess, and nonlinear base flow in the third soil layer. The model simulates surface water balance terms such as evapotranspiration, surface runoff, baseflow (subsurface drainage into the local stream channel network, as opposed to groundwater recharge), and total soil moisture in each soil layer. The critical elements in the VIC model that are particularly relevant to implementation in cold regions include: (a) a two-layer energy-balance snow model (Cherkauer & Lettenmaier, 1999), which is applied to non-glacierized areas and represents snow accumulation and ablation on both the ground and the overlying forest canopy where present; (b) a frozen soil/permafrost algorithm (Cherkauer & Lettenmaier, 1999, 2003) that solves for soil ice content within each vegetation type and represents the effects of frozen soils on the surface energy balance and runoff generation. A more complete description of the physics and applications of the VIC model can be found from the VIC homepage (https://vic.readthedocs.io/en/master/). The improved VIC (termed as VIC-glacier) has been successfully used in the upstream basin of major rivers in the Tibetan Plateau for flow simulation and prediction (Kan et al., 2018; Meng et al., 2019; Su et al., 2016; Sun & Su, 2020; Tong et al., 2016; Zhang et al., 2013; Zhao et al., 2015). Here, the VIC-glacier model was implemented at a 1/12° (~10 km) spatial resolution and a three-hourly time step. Glacier runoff here is defined as all water that originates from the glacierized area, including rainfall, snow melt, and ice melt. The simulated total runoff in each grid cell can be expressed as:

$$R_i = f \times R_{glac} + (1 - f) \times R_{vic} \quad (1)$$

where R_i is the total runoff (mm) in grid i; f is the percentage of glacier area (%) in grid i; R_{vic} is the runoff (mm) from non-glacierized area calculated by the VIC model (the sum of surface runoff and baseflow), which

is divided into rainfall and seasonal snowmelt runoff by subtracting standard VIC output of snowmelt from R_{vic}; R_{glac} is runoff (mm) from glacierized area composed of rainfall runoff, and snow and ice melt calculated with a temperature-index model. The glacierized area in each grid (when $f > 0$) is divided into different elevation bands to account for the topography influence on the temperature over glaciers (Kan et al., 2018). For each elevation band j:

$$M_j = \begin{cases} DDF \times T_j; & T_j > 0 \\ 0; & T_j \le 0 \end{cases} \quad (2)$$

$$R_{glac} = M_1 + \cdots + M_j;\ \mathrm{i} = 1, 2, 3, \ldots, \mathrm{n} \quad (3)$$

where, M_j is the meltwater (mm) from elevation band j and n is the total number of elevation bands in grid i; DDF is the degree-day factors of glacier or snow melt (mm C^{-1} day^{-1}); T_j (°C) is the daily average air temperature of elevation band j above the glacier surface. Here, the maximum temperature for snowfall and the minimum temperature for rainfall are usually set to +0.5°C and −0.5°C, respectively, consistent with that in the VIC model (Gao et al., 2010). The degree-day approach used here first melts snow on top of the ice with different degree-day factors for snow and ice surfaces to compute meltwater from a glacier band. The volume-area scaling approach (Bahr et al., 1997, 2015) is used to update the glacier area and volume every year with information on snow accumulation and simulated ice melt over the glacier. Runoff components (rainfall, snowmelt, and glacier runoff) from each grid cell are separately routed to the basin outlet through a channel network (Lohmann et al., 1998) to obtain daily discharge (m^3/s). The input data of the VIC-glacier model include gridded daily meteorological data (precipitation, maximum and minimum temperature, and wind speed), soil texture, vegetation types, and the initial percentage of glacier area for each grid cell (Table S3 in Supporting Information S1).

The VIC-Glacier model generally depends on two categories of parameters: (a) the parameters of the VIC model for simulating runoff in non-glacierized areas; and (b) the $DDFs$ (mm $°C^{-1}$ day^{-1}) of snow (DDF_{snow}) and glaciers (DDF_{ice}) to calculate meltwater from glacier surfaces. The DDF_{snow} was determined by the relationship between DDF_{snow} and DDF_{ice} ($DDF_{ice} = t \times DDF_{snow}$, where t is a scaling factor usually between 1.3 and 2.9) (Kumar et al., 2016; Singh et al., 2000). The VIC model parameters that require calibration are very limited, mostly including the infiltration shape parameter (b_{inf}), the depth of the first and second soil layers ($d1$ and $d2$), and three base flow parameters (D_s, W_s, and D_{smax}). The parameter b_{inf}, with a typical range of 0–0.4, defines the shape of the variable infiltration capacity curve. The first soil depth ($d1$) for each grid is usually set to 5–10 cm, as in Liang et al. (1996). The three baseflow parameters determine how quickly the water in the third layer ($d3$) evacuates and are generally less sensitive than parameters b_{inf} and $d2$. Consequently, only the infiltration-shape parameter (b_{inf}) and the second soil layer depth ($d2$) are targeted for calibration. The model calibration and validation were conducted using a two-step approach to overcome equifinality problems. First, parameters related to glacier melt were constrained using observed glacier area or glacier mass balance change data (Figure S4 in Supporting Information S1). Second, the VIC related parameters were calibrated and validated to observed streamflow (Figures S6 and S7 in Supporting Information S1). We further evaluated the VIC-glacier model simulations by comparing the VIC-simulated Snow Cover Fraction (SCF) and the Moderate Resolution Imaging Spectroradiometer (MODIS)-estimated SCF (Figure S8 in Supporting Information S1). The Nash-Sutcliffe efficiency (NSE), relative error (Er, %), and correlation coefficient (CC) were used for describing the prediction skill of the modeled variables. The details on the VIC-Glacier model calibration and validation are provided in Text S2 in Supporting Information S1. The constrained VIC-glacier model (in both climate inputs and model parameters), provides reliable current hydrological simulations with which to interpret the current runoff regime and response to future climate changes.

3.2.2. GCM Data and Downscaling

We used the outputs of monthly precipitation and temperature from 22 GCMs in the CMIP5 (Table S7 in Supporting Information S1) under RCP4.5 and RCP8.5 to generate the 21st century climate change scenarios for the four study basins. The raw monthly GCM outputs for 2006–2099 were downscaled and bias corrected to transient daily temperature and precipitation timeseries with respect to the historical reference data of 1961–2005 (1980–2005 for the upper Indus) by using the Bias Corrected Spatial Disaggregation (BCSD) statistical downscaling approach (Wood et al., 2002, 2004). The BCSD approach originated from the requirement to downscale ensemble climate

model forecasts as input to a macro-scale hydrologic model (like VIC) to produce flow forecasts at spatial and temporal scales appropriate for water management (Wood et al., 2002). The BSCD has been extensively used with the VIC model (Mote & Salathé, 2010; Salathé, 2005, 2007; Shrestha et al., 2014, 2015; Werner, 2011). For a detailed description on the BSCD, we refer to Werner (2011). Here, the bias correction and downscaling were performed in three steps: (a) The 22 GCMs and historical reference data (1961/1980–2005) were first aggregated to 1° × 1° grids, and then the bias correction of monthly GCM fields was conducted using quantile mapping relationships developed on the basis of the reference climate data and GCM-simulated historical precipitation and temperature for the overlapping period; (b) The bias-corrected monthly fields were disaggregated to the VIC-glacier model resolution (1/12° × 1/12°) using the "local scaling" of the corrected fields to the VIC-glacier model grids; and (c) the monthly fields were temporally disaggregated to daily resolution through resampling the daily historic record (at 1/12° × 1/12° scale) conditioned on the monthly averages of the locally scaled fields. The above bias correction and downscaling procedure were conducted at each grid and each month for all the GCMs and scenarios. After the downscaling and bias-correction process, each basin had 94 years (2006–2099) of daily transient climate projections under 44 scenarios (22 GCMs × 2 RCPs) (Figure S9 in Supporting Information S1), which were directly used to drive the VIC-glacier model to produce continuous runoff and streamflow projections over each basin.

3.2.3. Extreme Flow Indices

For high flow, we used the annual maximum daily discharge as the index for floods (Boulange et al., 2021; Hirabayashi et al., 2013). We focused on analyzing the change in magnitude of maximum discharge with return periods of 10, 50, and 100 years. The simulated daily discharge maxima were first ranked in ascending order and fitted to the Pearson Type III distribution using the L-moment method (Hosking, 1990; Vogel & Wilson, 1996). The evolution of the maximum daily discharge corresponding with events that occur once in 10, 50, and 100 years was obtained with a 30-year moving window from 1970 (1980 for the UI) to 2099 for each GCM, scenario, and basin.

For low flow, first we determined a threshold based on the simulated daily streamflow in historical periods (1965/1980–2005) for each basin using the 80% exceedance frequency of the flow duration curves (i.e., flow i.e., exceeded 80% of the time), commonly used in the analysis of low flow frequencies (Fleig et al., 2006; Heudorfer & Stahl, 2017). The threshold was calculated for each day in a year; therefore, a set of 365 80th-percentile threshold values were generated at the outlets of each basin based on the daily flow data in historical periods (Figure S10 in Supporting Information S1). Second, based on the 80th-percentile daily flow thresholds, we used annual maximum consecutive drought days (CDD) and annual total pooled deficit volume (PDV) to measure the evolution of potential streamflow drought (defined as below-normal streamflow) (Feyen & Dankers, 2009; Fleig et al., 2006; Sarailidis et al., 2019) prior to the end of the 21st century. The maximum CDD was defined as the maximum consecutive days within a year when daily streamflow remains below the 80th-percentile daily flow thresholds, and the annual PDV was defined as annual accumulated streamflow deficit to the 80th-percentile thresholds within a year. Both the annual maximum CDD and annual PDV were continuously calculated for each GCM, scenario, and basin from 1970/1980 to 2099.

4. Results

4.1. Current Flow Regime

Although precipitation in all of these basins is dominated by westerly winds, they each show distinct precipitation and runoff regimes (Figure 1) largely associated with differing basin morphology (Table 1). In the USD (glacier coverage of 0.9%), seasonal snowmelt (41%) and rainfall (49%) dominate the flow regime with flow peaks in late spring and early summer (May-July). The annual contribution of glacier runoff (defined as all water that runs off from glacier areas) is limited (about 10% of annual total), but it plays an important role in the relatively dry summer months (18%–32% of monthly total flow in July-September) (Figure 1 and Table S5 in Supporting Information S1). In the UAD (glacier coverage of 3.3%), runoff is also strongly influenced by seasonal snow (31%) and to a greater extent by glacier runoff (24%), with an initial runoff peak in spring from snowmelt and rainfall and a second peak in summer from glacier melt (accounting for 41%–57% of total flows in July-September, when precipitation is lowest). The UYK (glacier coverage of 9.3%) has a precipitation maximum in summer, but runoff is dominated by glaciers that contribute 52% of the annual total and 72% in July-August, when river flow peaks.

In the UI (glacier coverage of 11.9%), precipitation peaks twice, in winter-spring and in summer (Figure 1), due to the combined influences of the westerlies and the Indian Summer Monsoon. River discharge peaks in July-August mainly due to seasonal snowmelt and rainfall runoff (61%–72%) (Figure 1). Forced by bias-corrected precipitation (Text S1 in Supporting Information S1), our model estimates a glacier contribution of 22% of the annual runoff total and 28%–38% of the July–August total in the UI. This is less than previous model estimates of 40%–48% (Lutz et al., 2014; Zhang et al., 2013) (Table S1 in Supporting Information S1) using gauge-based APHRODITE precipitation subsequently found to be underestimated (Dahri et al., 2016, 2018; Immerzeel et al., 2015), but larger than the model estimates of 5.1%–11.5% using the ERA-interim or ERA5 reanalysis precipitation (Khanal et al., 2021; Wijngaard et al., 2017) (Table S1 in Supporting Information S1). An underestimation of precipitation input can be compensated for by an overestimation of meltwater when calibrated to discharge data, and vice versa (Pellicciotti et al., 2012; Sun & Su, 2020), suggesting the high importance of accurate precipitation input in acquiring a correct flow composition and runoff regime.

4.2. Future Climate and Flow Evolution

Significant warming, at 0.22–0.46°C/10a, persists from the present to the projected future (from 2006 to 2099) in all basins (Figure S9 in Supporting Information S1), with a much larger spread between RCPs in the second half of the century. This increased spread results from a reduced warming rate in RCP4.5 (at 0.15 ± 0.07°C/10a to 0.23 ± 0.13°C/10a, multi-GCM mean ± 1 standard deviation) and accelerating warming in RCP8.5 (0.58 ± 0.17°C/10a to 0.80 ± 0.22°C/10a) (Table S6 in Supporting Information S1). Precipitation is projected to increase (with larger uncertainties than for temperature) in the UI and UYK, with greater rates of increase in the second half of the century for RCP8.5 (6.8 ± 8.01 mm/10a to 9.4 ± 13.7 mm/10a). In contrast, the USD and UAD exhibit little trend in projected precipitation (0.4 ± 4.2 mm/10a to 1.3 ± 3.5 mm/10a in 2006–2099) and little difference between RCPs (Table S6 in Supporting Information S1).

The distinct runoff regimes of the studied basins largely determine their basin response to future climate change (Figure 2), although some common characteristics in their responses are apparent. There is a broadly consistent increase in rainfall runoff and decrease in snowmelt runoff throughout the 21st century (Figures S11 and S12 in Supporting Information S1) as a result of more precipitation falling as rain instead of snow each year (Figure S14 in Supporting Information S1), a phenomenon also reported in other snow-dominated regions in a warming world (Barnett et al., 2005; Bintanja & Andry, 2017; Livneh & Badger, 2020). There is also a general decline or slowing increase in glacier runoff (Figure S13 in Supporting Information S1) in the second half of the century under RCP4.5 associated with the shrinking glacier area (Figure S15 in Supporting Information S1) and a reduction in the warming rate after 2040–2050.

In the first half of the 21st century, mean annual total runoff increases in all basins under both RCPs (by 2.4 ± 6.4 to 21.2 ± 10.8 mm/10a) (Figure 2 and Table S6 in Supporting Information S1), but the drivers of these runoff increases differ between basins and, in some cases, between RCPs. Rainfall dominates runoff increases under both RCPs in the USD (Figures S11–S13 in Supporting Information S1), and contributes >85% of runoff increases (by 13 ± 14%) in 2020–2049 relative to 1971–2000 mean. In the UAD and UYK, however, this is only the case under RCP4.5. Under RCP8.5, glacier melt dominates the increases in runoff in the UAD, UYK and UI, with runoff increases of 9 ± 12%, 29 ± 11% and 15 ± 7% respectively, relative to 1971–2000 (Tables S8–S11 in Supporting Information S1). Most notably, ~80% of the increase in UI mean annual runoff is driven by an increase in glacier melt.

In the second half of the century (Figure 2), under RCP4.5 total runoff stabilizes or declines in all basins except the UI as increases in rainfall runoff are counterbalanced by declining snow and glacier runoff. In the UI, however, glacier runoff and total runoff continue to increase (Figure 3 and Figure S13 in Supporting Information S1). Under RCP8.5 this contrast is more pronounced, with mean annual runoff in the USD, for example, changing little (decreasing by 2.1 ± 4.8 mm/10a) (Table S6 in Supporting Information S1) as rainfall gains are largely balanced by reduced glacier melt (Figures S11–S13 in Supporting Information S1), while in the UI, glacier melt drives a rapid ongoing rise in total runoff (at 32.5 ± 12.4 mm/10a) in response to both precipitation and temperature increases and limited glacier retreat (18% by area at the end of the century, Figure S15 in Supporting Information S1). By the end of the 21st century, UI glacier runoff continues to rise, contributing about 77% of the total UI runoff increase in 2070–2099 (of 49 ± 17% for RCP8.5) (Table S11 in Supporting Information S1). Total runoff in the UAD and UYK also rises under RCP8.5, driven by increases in both rainfall and glacier runoff

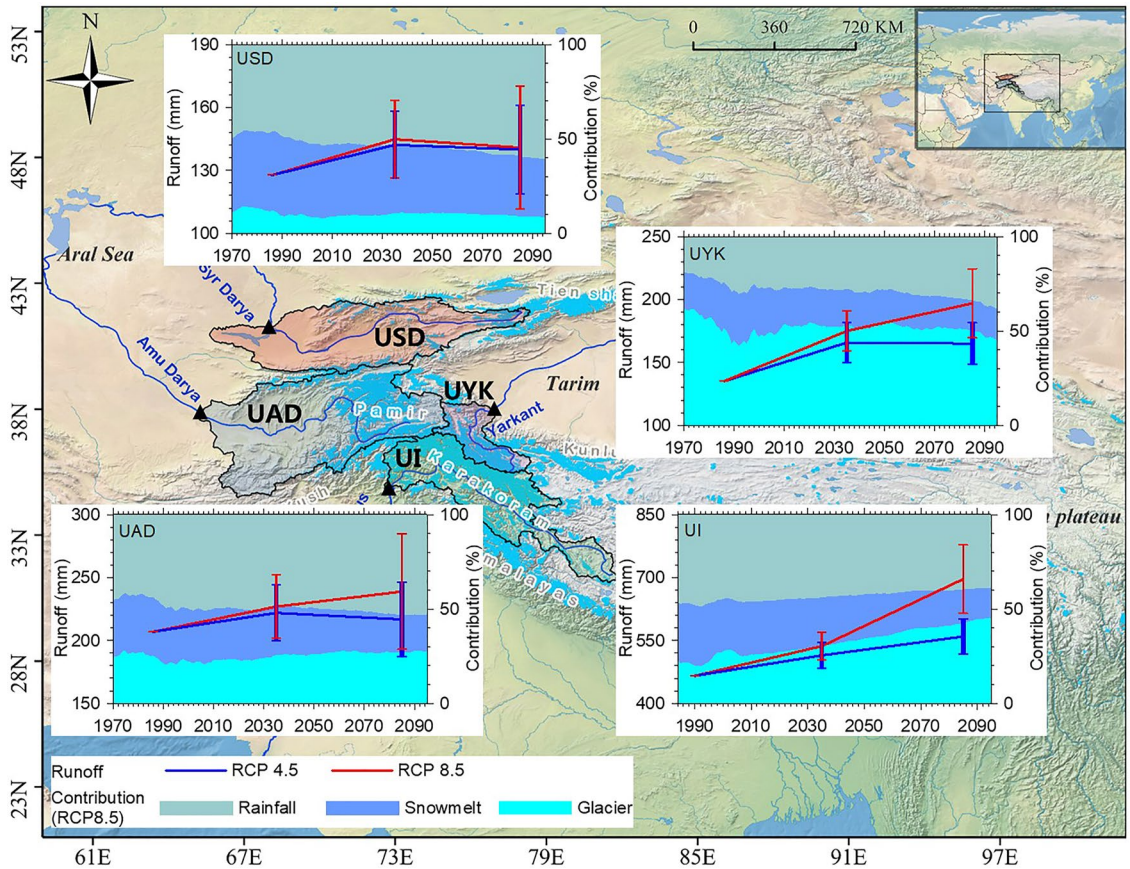

Figure 2. Projected annual flow composition (%, right *y*-axis) in the four upper basins in the 21st century under RCP8.5, and total runoff (mm, left *y*-axis) in the reference period (1971–2000/1980–2000), near future (2020–2049) and far future (2070–2099) under RCP4.5 and RCP8.5. Solid lines represent the ensemble means of 22 downscaled hydrological model runs for the four upper basins (USD: Syr Darya; UAD: Amu Darya; UYK: Yarkant; UI: Indus). The errors bars denote one standard deviation.

in the UAD and predominantly rainfall in the UYK, where glacier runoff declines as glaciers retreat in the latter half of the century (by 62% in area, Figures S13 and S15 in Supporting Information S1).

Rainfall runoff supplies an increasingly large fraction of total runoff in all basins except the UI, especially in the second half of the century (Figure 2). This is particularly notable in the USD, however, as it shifts from a rain-snow regime in the first half of the century to a more rainfall-dominated regime in the second. In the UAD and UYK, glacier runoff remains a substantial but ultimately declining water resource throughout this century. Glaciers contribute about 23%–30% of UAD total runoff and as much as 44%–49% of UYK totals in 2070–2099. Here also though, rainfall plays an increasingly important role, contributing 55%–69% of the total flow increase under RCP8.5 between the periods 1971–2000 and 2070–2099 in UAD (of 15 ± 22%) and in UYK (of 46 ± 20%) (Tables S8–S11 in Supporting Information S1).

4.3. Future Flow Seasonality

The warming climate is expected to reduce snowfall and shift the snowmelt season earlier (Barnett et al., 2005; Kraaijenbrink et al., 2021; Musselman et al., 2018). This is especially the case in the more snowmelt-dependent USD and UAD basins (Figure 3). In the USD, we project increasing spring runoff (by 27 ± 13 to 80 ± 40% relative to 1971–2000) and a peak one month earlier (shifting from June to May) in both the near (2020–2049) and farther future (2079–2099) under both RCPs (Figure 3 and Table S8 in Supporting Information S1). This seasonal shift, in conjunction with a general reduction in summer precipitation (Figure S17 in Supporting Information S1) and the reduced buffering role from glaciers, results in relatively large decreases in USD summer river flow toward the end of the century (e.g., by 16 ± 13 to 30 ± 17% in July-September), leaving the relatively dry USD summers even drier.

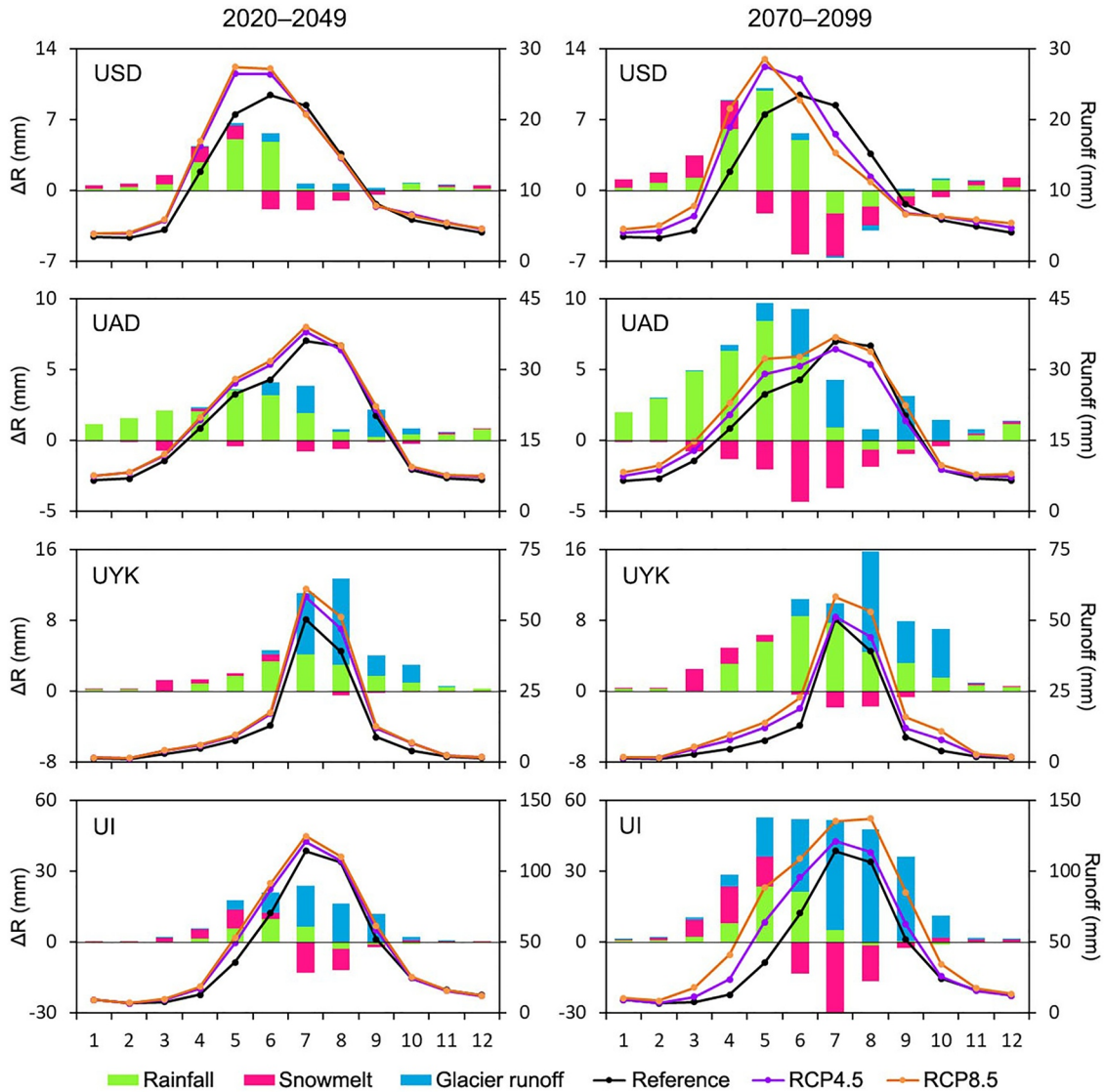

Figure 3. Monthly average of total runoff in near future (2020–2049) and far future (2070–2099) and the change in their runoff components relative to the reference period. The dotted solid lines represent simulated mean monthly total runoff for the reference period 1971–2000 (1980–2000 for the UI) and the projections for periods 2020–2049 and 2070–2099, based on the ensemble means of 22 hydrological simulations under two RCPs (RCP4.5 and RCP8.5) in the four upper basins (USD: Syr Darya; UAD: Amu Darya; UYK: Yarkant; UI: Indus). The bar plots indicate the mean seasonal changes in rainfall, snowmelt, and glacier runoff under RCP8.5 relative to the reference period.

In contrast, in the UAD (Figure 3 and Table S9 in Supporting Information S1) the timing and magnitude of peak flow changes little under both RCPs by the end of century. Changes are within ±2% for July-August for RCP8.5, despite enhanced spring runoff (by 30 ± 34 to 38 ± 44% relative to 1971–2000), largely because glacier runoff still provides a primary water source in the dry seasons toward the end of the century (supplying 49%–60% of July-September totals under RCP 8.5).

More strikingly, in the most-glacierized UI and UYK (Figure 3 and Table S10–S11 in Supporting Information S1), we project changes in the opposite direction, with substantial river-flow increases in summer by both 2020–2049 and 2070–2099, and largely unchanged seasonal regimes. In the UI, the end-of-century under RCP8.5 stands out, with flow increases year-round and an increase of 18 ± 16 to 65 ± 33% in July-September, primarily driven by enhanced glacier runoff under the substantially warmer climate and increased precipitation of 2070–2099 (Figures S16 and S17 in Supporting Information S1). In the UYK, the largest flow increases for 2020–2049 appear in July-August (by 16 ± 11 to 31 ± 13%) in both RCPs, with glacier runoff the dominant

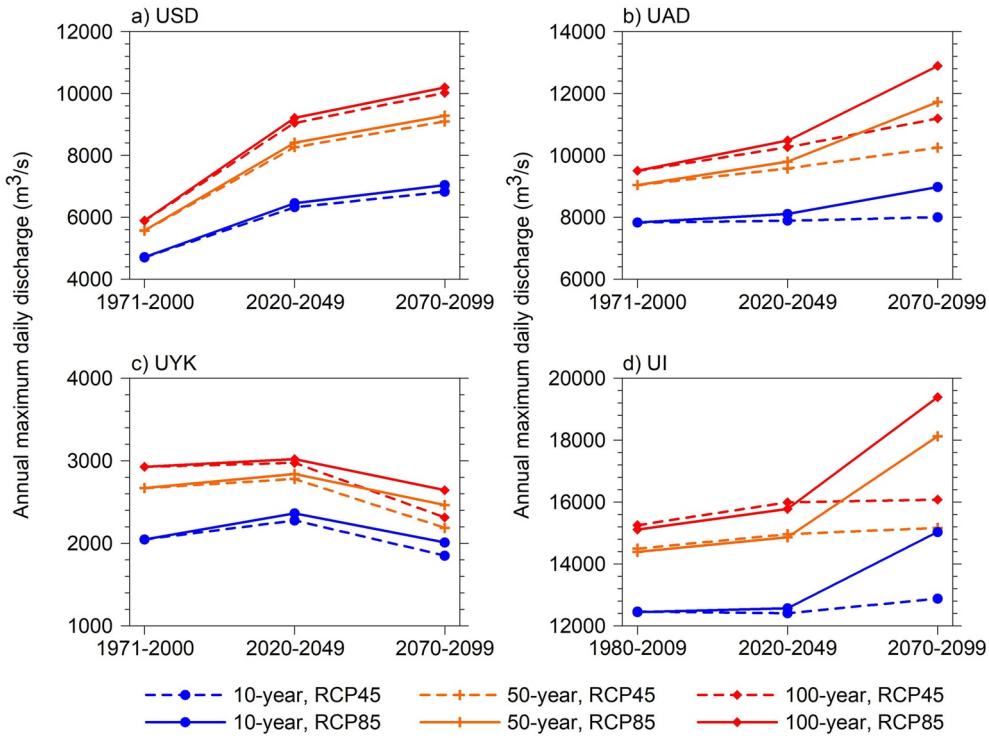

Figure 4. Annual maximum daily discharge corresponding to 10-year, 50-year, and 100-year return periods under RCP4.5 and RCP8.5. The figure shows three 30-year windows including the reference (1971–2000/1980–2009) and two future periods (2020–2049 and 2070–2099) based on the ensemble mean of 22 transient runs for each RCP at the outlets of the four upper basins (black triangles in Figure 1).

contributor (55%–80%). In the late century for RCP8.5, the early summer rainfall contribution increases (contributing 96% of flow increase in July), along with enhanced glacier runoff accounting for 66%–81% of increased water availability in August and the dry months of September and October.

4.4. Future Flow Extremes

As with the annual and seasonal runoff changes described above, strong contrasts between basins exist in the projected wet and dry extremes of river flow. Superimposed on the substantially drier summer mean runoff anticipated in the USD (Figure 3), multi-model means suggest particularly strong increases in the severity of both extreme high and low river-flow events in this basin under both RCPs. At the wet extreme, the annual-maximum daily discharge at 10-year, 50-year, and 100-year return periods increases in magnitude through the 21st century (Figure 4a), although uncertainty ranges are large (Figure S18 in Supporting Information S1). Relative to 1971–2000, the 2070–2099 daily maximum under RCP8.5, for example, is projected to increase by 67% (20%–130% among the 22 GCMs) and 73% (26%–142% among the 22 GCMs) for the 50-year and 100-year occurrence intervals respectively (Figure 4a). The maximum discharge also tends to occur earlier in future periods (Figure S19a in Supporting Information S1), which can be explained by the projected earlier snow melt and increase in rainfall runoff (Figure 3). Alongside this, however, at the dry extreme, both the annual maximum consecutive drought days (CDD) and the total pooled deficit volume (PDV) also increase strongly in the USD, particularly in the latter half of the century (Figure 5a). Relative to 1971–2000, the 2070–2099 mean annual maximum CDD under RCP8.5 is projected to increase by 39 days (−14 to +137 days among the 22 GCMs) and total PDV to increase by 458% (−61 to +2024% among the 22 GCMs). The mean annual maximum CDD will likely also shift from late spring (April–May) in 1971–2000 to mid-summer (July) in future (Figure S19b in Supporting Information S1), which can be related to the projected seasonal runoff shifts in the USD (Figure 3).

In the UI, UAD and UYK, the maximum daily discharge also increases, but by smaller relative amounts. In the most-glacierized UI, the daily maximum is projected to increase for all return periods (Figure 5d), with

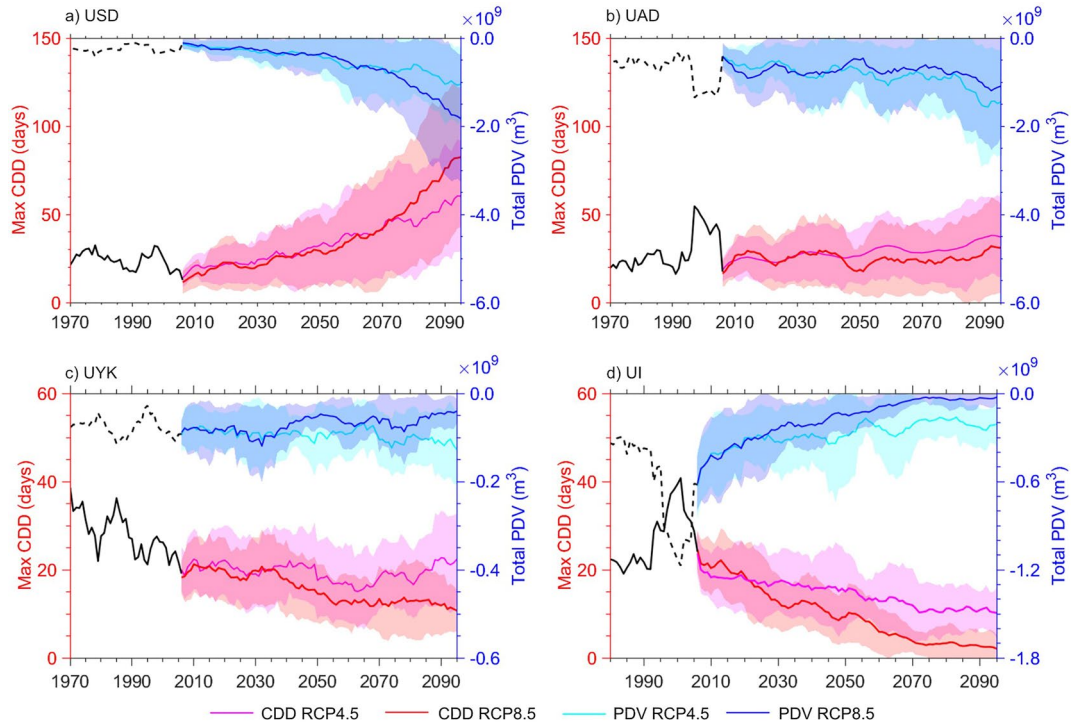

Figure 5. Annual maximum consecutive drought days and total pooled deficit volume from present to the end of the 21st century. Solid lines for projection periods (2006–2099) represent the ensemble means of hydrological model results driven by 22 GCMs for each year, each RCP, and each basin. The shadings denote one standard deviation among the 22 GCMs runs.

considerably greater increases after 2050 under RCP8.5 than under RCP4.5. The 50-year maximum, for example, is projected to increase by 5% (−20 to +55% among the 22 GCMs) under RCP4.5 but 26% (6%–81%) under RCP8.5 by the end of the century. Glacier melt inputs largely determine the intensity and frequency of extreme high flows at all return periods (Figures S20 and S21 in Supporting Information S1). The general increase in high flows in the UI are in line with previous studies (Lutz et al., 2016; Wijngaard et al., 2017), however, large dicreprencies in magnitude exist due to the different climate scenarios and approaches used.

Similarly to the UI, the maximum daily discharges at all return periods in the UAD increase considerably more under RCP8.5 than RCP4.5 (Figure 5b), by up to 30% by the end of the 21st century, due to both projected increase in glacier and rainfall runoff (Figures S11 and S13 in Supporting Information S1). In the UYK, the daily maximum rises until around 2030–2040 followed by a decline for the rest of the 21st century for all return periods (Figure 5c), being highly regulated by the increase and then decrease in glacier runoff inputs (Figures S20 and S21 in Supporting Information S1).

At the dry extreme, changes in the duration and severity of low flows in the UI and UYK are in particular contrast to those in the USD. The annual maximum CCD and total PDV generally decrease under both RCPs for the UYK and particularly for the UI (Figure 5d), where glaciers play a strong summer buffering role. In the UAD, more modest and later increases than those in the USD are projected in maximum CDD and total PDV (by 45%–86% in 2070–2099, Figure 5b) under both RCPs.

5. Uncertainty

Although we have conducted multi-variable and multi-objective constraints on both climate input and model parameters, uncertainties and limitations remain which are mainly related to the scarcity of gauge observations and the simple representation of glacier melt processes. As the key driver of terrestrial hydrological cycle and glacier mass gains, precipitation accounts for a major uncertainty in flow composition and flow regime. Taking the most glacierized basins of the UI and UYK as examples (Figures S22a and S22b in Supporting Information S1), the glacier runoff contribution tends to increase with the decrease of precipitation (e.g., 40% decreases

in precipitation resulting in 15% and 29% increases in the glacier runoff contribution in the UI and UYK, respectively), while snowmelt and rainfall contributions tend to decrease with precipitation. In the several previous studies (Tables S1 and S2 in Supporting Information S1), the discrepancies in runoff composition can be largely explained by the varying magnitudes of precipitation inputs (e.g., ranging between 311 and 832 mm in the UI and 326–942 mm in the USD in annual means). Uncertainties resulting from the challenges/issues in precipitation inputs for model calibration and validation have been widely recognized and assessed in the TP region (Dahri et al., 2021; Lutz et al., 2014, 2016; Pellicciotti et al., 2012; Ragettli et al., 2013; Sun & Su, 2020; Wortmann et al., 2018). Therefore, developing a homogenized and representative climate data archive is urgently needed for a better understanding or assessment or quantification of current and future water availability in the TP.

Another important source of uncertainties in glacier runoff estimation is the determination of degree-day parameter DDF, which has considerably spatial and temporal variability (Hock, 2003; Rounce, Khurana, et al., 2020). In this work, debris-covered glaciers are not explicitly considered, which account for about 10% of the total glacierized area in the High Mountain Asian and may exert an important control on glacier ablation due to its lower albedo and insulation role at the same time (Kraaijenbrink et al., 2017; Shea et al., 2021). The DDF parameters in this study theoretically represent the average conditions for each basin. Sensitivity tests show that the absolute changes are about 1.3%–3.2% in average annual glacier runoff and 1.0% in its contribution, with the change of DDF_{ice} by one unit (mm $°C^{-1}$ day^{-1}) in the UYK and UI (Figures S22c and S22d in Supporting Information S1), much less than the uncertainties from precipitation inputs. However, the determination of the DDF largely relies on the initial glacier condition and glacier's area and/or mass change data used for calibration (Table S3 in Supporting Information S1), which are subject to large uncertainties (Nuimura et al., 2015; Sakai, 2019); any of the uncertainties can propagate into the future glacier runoff projections. Our projected evolution of glacier runoff is generally in line with Rounce, Hock, and Shean (2020) in the UYK, USD, and UAD (UI only for RCP4.5) who used glacier mass observations to constrain climate inputs and glacier model parameters, and with Wortmann et al. (2022) in the UYK, who used a corrected precipitation input and more complex glacier evolution model. The current glacier scheme has a lower complexity than the other processes in the VIC model, resulting in a weak interaction between the glacier and non-glacier areas within each grid. As more systematic observations of mass balance and glacier inventory data (Rounce, Hock, & Shean, 2020; Sakai, 2019) and satellite-based radiation and meteorological data become available in the TP, more physically based energy-balance glacier models (e.g., Hock & Holmgren, 2005) coupled with the process-based hydrological model that balances the physical realism of the model with its usability (e.g., Ren et al., 2018) are expected to better describe the hydrological consequences of climate and glacier changes spatiotemporally.

The uncertainty associated with the VIC model parameters is generally smaller than the uncertainty associated with the climate forcing (Figures S22e and S22h in Supporting Information S1). The changes of model relative error (Er) are within 8% when the infiltration parameter b_{inf} varies from 0.05 to 0.4 and the second soil layer depth (*d2*) from 0.5 to 3.0 m and the changes of NSE are generally within 0.1 in the UYK and UI. Since all VIC parameters were calibrated in terms of NSE and Er, the final parameters tend to have the highest NSE and lowest Er. However, the parameters are highly dependent on the precipitation data used for calibration. When the precipitation input changes, the parameters may change accordingly in order to match streamflow data, further emphasizing the extreme importance of accurate precipitation in acquiring reliable model parameters and simulations.

In addition, the considerable variations in future runoff projection primarily result from the large spread in the GCMs, especially in precipitation-dominated basins, since GCMs tend to have larger uncertainties in precipitation projections than in temperature (Figure S9 and Table S6 in Supporting Information S1). The uncertainty in the projected precipitation change (mm/10a), expressed by the standard deviation (SD) of 20 GCMs, is 1.2–1.5 times the ensemble means in the UYK and UI in the latter half of the 21st century, and is even much larger in the USD and UAD with the SD reaching 22–49 times the ensemble means (Table S6 in Supporting Information S1). The future runoff changes (mm/10a) exhibit the largest uncertainties in the USD and UAD basins (with SD of 24–35 times the ensemble mean), mostly associated with the largest precipitation uncertainty and its precipitation-dominated flow regime. Despite the large uncertainties in future climate and water availability, basin-wide patterns and trends of seasonal shifts and extreme flows are generally consistent among the GCMs.

At the time when we finished this manuscript, a certain number of CMIP6 models already became available, which are driven by alternative scenarios of emissions and land use changes based on the combinations of

Shared Socioeconomic Pathways (SSPs) and forcing pathways (Eyring et al., 2016; O'Neill et al., 2016; Stouffer et al., 2017). Our recent evaluation of 18 CMIP6 models over the Third Pole region (Li et al., 2021) suggest that, compared to CMIP5 models, the improvements in CMIP6 precipitation and temperature simulation are relatively marginal in this high mountain region, and the wetting and cold biases observed in CMIP5 (Su et al., 2013) are persisting in CMIP6 models. The precipitation and temperature projections under SSP2-4.5 and SSP5-8.5 show similar change directions in the 21st century to those under RCP 4.5 and RCP 8.5, respectively, in both monsoon and westerlies regions. But the CMIP6 models exhibit larger future warming rates than the CMIP5 in the Third Pole region (Li et al., 2021; Su et al., 2013), due to the already recognized heightened equilibrium climate sensitivity (ECS) in CMIP6 models (Voosen, 2019; https://www.carbonbrief.org/cmip6-the-next-generation-of-climate-models-explained). Therefore, our projected summer drought and wet and dry extremes under RCP4.5 and RCP8.5 here, are expected to become even more severe under the corresponding CMIP6 emission scenarios in these western TP basins.

6. Summary and Implications

In this study we systematically quantify the contemporary flow regime and future evolution of total water availability, seasonal shifts, and dry and wet discharge extremes in the four upper mountain basins in the western TP. In summary, our analysis illustrates contrasting patterns of hydrological response to projected climate changes in the 21st century across the four basins, dictated by their varying present-day climate and hydrological regimes. In the first half of 21st century, total water supply from these headwaters is projected to increase in all basins, with increases primarily driven by increased rainfall in the USD and enhanced glacier melt in the upper Indus, and by both inputs in the UAD and Yarkant. In the upper Indus, enhanced glacier runoff will sustain this increase in summer water supplies through the second half of this century, considerably decreasing the severity of seasonal water shortages but considerably increasing the flood hazard, particularly under RCP8.5. In the UYK and UAD, the seasonal regimes will remain largely unchanged and total water supply is likely to keep increasing under the rather extreme emissions scenario RCP8.5 through the second half of the 21st century, as glaciers continue to provide a primary water source in summer months. In stark contrast, the USD will face a declining annual water supply and considerably greater hazard from both extreme spring floods and summer water shortages in the second half of the century under both RCPs, as its glaciers retreat and snowmelt arrives earlier in the spring.

The Syr Darya's reduced mean summer water supply and more severe hydrological droughts are likely to exacerbate ongoing water stress and conflicts over seasonal water allocation among the Syr Darya's riparian countries (Bernauer & Siegfried, 2012; Siegfried et al., 2011; Sorg et al., 2014; Unger-Shayesteh et al., 2013), notably in unregulated catchments in the summer months, when water demand for irrigation is at its greatest. These additional stresses will be superimposed on a background of rising regional demand as Central Asia's population is projected to grow by about 40 million (or 55% increase) relative to 2020 by the end of the century, with Uzbekistan contributing 22% and Tajikistan 39% to this growth (United Nations, 2019). This suggests that the need for mitigation and adaptation strategies, such as improving the water storage capacity and resource allocation mechanisms through the strengthening of transboundary institutions, will be ever more urgently needed in this water-stressed and conflict-prone region (Bernauer & Siegfried, 2012; Sorg et al., 2014). However, the threat of more extreme future flood regimes in the Syr Darya, Amu Darya, and Indus imply that the costs and challenges involved in building and maintaining water-management infrastructure will be substantially greater than they are today.

Although these four basins exhibit a variety of hydrological responses to 21st century climate change, a key common theme is the progressive loss of snow and ice from the mountain cryosphere, driven primarily by rising temperatures. This cryospheric resource plays a critical role in sustaining runoff to the downstream basins during the spring and summer growing seasons, when water is at its most valuable to society and when shortages are most damaging (Pritchard, 2019). Starting with the smallest glacier extent and contribution to runoff (Table 1 and Figure 2), the Syr Darya basin is making the earliest transition from a hydrological regime buffered by snow and ice to a more volatile pluvial regime. However, the same transition is also underway in the other three basins (Kraaijenbrink et al., 2017), and this is important because it is considerably more difficult for society to adapt to a more volatile water supply than to a changing average supply (Hall et al., 2014). For the population of these basins and the broader region, it would therefore be very beneficial to protect this resource by pursuing a low-emissions climate pathway that minimizes further warming in the TP.

Data Availability Statement

Glacier data were from the Randolph Glacier Inventory RGI V4.0 and RGI V6.0 (http://www.glims.org/RGI/), and the First and Second Glacier Inventory of China (http://www.tpdc.ac.cn/zh-hans/). Snow cover fraction data were from the Moderate Resolution Imaging Spectroradiometer (MODIS)10C2 (https://nsidc.org/data). Topography data were from the Shuttle Radar Topography Mission (SRTM3) DEM (https://www2.jpl.nasa.gov/srtm/). Global land cover map was obtained from the University of Maryland (https://glad.umd.edu/dataset). Soil data were from Global Soil Data Products CD-ROM Contents (IGBP-DISIGBP-DIS) (http://dx.doi.org/10.3334/ORNLDAAC/565). Streamflow data were from Interstate Commission for Water Coordination of Central Asia, Water and Power Development Authority of Pakistan, and Xinjiang Hydrology Bureau. The corrected gridded precipitation can be found in the National Tibetan Plateau/Third Pole Environment Data Center (http://data.tpdc.ac.cn/en/), and are also immediately available from the corresponding author upon reasonable request.

Acknowledgments
This work was financially supported by National Natural Science Foundation of China (41988101, 41871057) and the Second Tibetan Plateau Scientific Expedition and Research Program (2019QZKK0201). The authors thank Daqing Yang and Yi Luo for their constructive comments on this work.

References

Alford, D., Kamp, U., & Pan, C. (2015). *The role of glaciers in the hydrologic regime of the Amu Darya and Syr Darya basins*. World Bank. Retrieved from https://openknowledge.worldbank.org/handle/10986/24082

Bahr, D. B., Meier, M. F., & Peckham, S. D. (1997). The physical basis of glacier volume-area scaling. *Journal of Geophysical Research*, *102*(B9), 20355–20362. https://doi.org/10.1029/97JB01696

Bahr, D. B., Pfeffer, W. T., & Kaser, G. (2015). A review of volume-area scaling of glaciers. *Reviews of Geophysics*, *53*(1), 95–140. https://doi.org/10.1002/2014RG000470

Baldwin, J., & Vecchi, G. (2016). Influence of the Tian Shan on arid extratropical Asia. *Journal of Climate*, *29*(16), 5741–5762. https://doi.org/10.1175/JCLI-D-15-0490.1

Barnett, T. P., Adam, J. C., & Lettenmaier, D. P. (2005). Potential impacts of a warming climate on water availability in snow-dominated regions. *Nature*, *438*(7066), 303–309. https://doi.org/10.1038/nature04141

Bernauer, T., & Siegfried, T. (2012). Climate change and international water conflict in Central Asia. *Journal of Peace Research*, *49*(1), 227–239. https://doi.org/10.1177/0022343311425843

Bhattacharya, A., Bolch, T., Mukherjee, K., King, O., Menounos, B., Kapitsa, V., et al. (2021). High Mountain Asian glacier response to climate revealed by multi-temporal satellite observations since the 1960s. *Nature Communications*, *12*(1), 4133. https://doi.org/10.1038/s41467-021-24180-y

Biemans, H., Siderius, C., Lutz, A. F., Nepal, S., Ahmad, B., Hassan, T., et al. (2019). Importance of snow and glacier meltwater for agriculture on the Indo-Gangetic Plain. *Nature Sustainability*, *2*(7), 594–601. https://doi.org/10.1038/s41893-019-0305-3

Bintanja, R., & Andry, O. (2017). Towards a rain-dominated Arctic. *Nature Climate Change*, *7*(4), 263–267. https://doi.org/10.1038/nclimate3240

Blöschl, G., Hall, J., Parajka, J., Perdigão, R. A. P., Merz, B., Arheimer, B., et al. (2017). Changing climate shifts timing of European floods. *Science*, *357*(6531), 588–590. https://doi.org/10.1126/science.aan2506

Bolch, T., Kulkarni, A., Kääb, A., Huggel, C., Paul, F., Cogley, J. G., et al. (2012). The state and fate of Himalayan glaciers. *Science*, *336*(6079), 310–314. https://doi.org/10.1126/science.1215828

Boulange, J., Hanasaki, N., Yamazaki, D., & Pokhrel, Y. (2021). Role of dams in reducing global flood exposure under climate change. *Nature Communications*, *12*(1), 417. https://doi.org/10.1038/s41467-020-20704-0

Braun, L. N., Weber, M., & Schulz, M. (2000). Consequences of climate change for runoff from Alpine regions. *Annals of Glaciology*, *31*, 19–25. https://doi.org/10.3189/172756400781820165

Cannon, F., Carvalho, L. M. V., Jones, C., & Norris, J. (2016). Winter westerly disturbance dynamics and precipitation in the Western Himalaya and Karakoram: A wave-tracking approach. *Theoretical and Applied Climatology*, *125*(1–2), 27–44. https://doi.org/10.1007/s00704-015-1489-8

Chen, Y. N., Li, W. H., Xu, C. C., & Hao, X. M. (2007). Effects of climate change on water resources in Tarim River Basin, Northwest China. *Journal of Environmental Sciences*, *19*(4), 488–493. https://doi.org/10.1016/S1001-0742(07)60082-5

Chen, Y. N., Li, Z., Fang, G. H., & Li, W. H. (2018). Large hydrological processes changes in the transboundary rivers of central Asia. *Journal of Geophysical Research: Atmospheres*, *123*(10), 5059–5069. https://doi.org/10.1029/2017JD028184

Cherkauer, K. A., & Lettenmaier, D. P. (1999). Hydrologic effects of frozen soils in the upper Mississippi River basin. *Journal of Geophysical Research*, *104*(D16), 19599–19610. https://doi.org/10.1029/1999JD900337

Cherkauer, K. A., & Lettenmaier, D. P. (2003). Simulation of spatial variability in snow and frozen soil. *Journal of Geophysical Research*, *108*(D22), 8858. https://doi.org/10.1029/2003JD003575

Dahri, Z. H., Ludwig, F., Moors, E., Ahmad, B., Khan, A., & Kabat, P. (2016). An appraisal of precipitation distribution in the high-altitude catchments of the Indus basin. *Science of the Total Environment*, *548–549*, 289–306. https://doi.org/10.1016/j.scitotenv.2016.01.001

Dahri, Z. H., Ludwig, F., Moors, E., Ahmad, S., Ahmad, B., Shoaib, M., et. al. (2021). Spatiotemporal evaluation of gridded precipitation products for the high-altitude Indus basin. *International Journal of Climatology*, *41*(8), 4283–4306. https://doi.org/10.1002/joc.7073

Dahri, Z. H., Moors, E., Ludwig, F., Ahmad, S., Khan, A., Ali, I., & Kabat, P. (2018). Adjustment of measurement errors to reconcile precipitation distribution in the high-altitude Indus basin. *International Journal of Climatology*, *38*(10), 3842–3860. https://doi.org/10.1002/joc.5539

De Stefano, L., Petersen-Perlman, J. D., Sproles, E. A., Eynard, J., & Wolf, A. T. (2017). Assessment of transboundary river basins for potential hydro-political tensions. *Global Environmental Change*, *45*, 35–46. https://doi.org/10.1016/j.gloenvcha.2017.04.008

Duethmann, D., Bolch, T., Farinotti, D., Kriegel, D., Vorogushyn, S., Merz, B., et al. (2015). Attribution of streamflow trends in snow and glacier melt-dominated catchments of the Tarim River, Central Asia. *Water Resources Research*, *51*(6), 4727–4750. https://doi.org/10.1002/2014WR016716

Duethmann, D., Menz, C., Jiang, T., & Vorogushyn, S. (2016). Projections for headwater catchments of the Tarim River reveal glacier retreat and decreasing surface water availability but uncertainties are large. *Environmental Research Letters*, *11*(5), 054024. https://doi.org/10.1088/1748-9326/11/5/054024

Eyring, V., Bony, S., Meehl, G. A., Senior, C. A., Stevens, B., Stouffer, R. J., & Taylor, K. E. (2016). Overview of the Coupled Model Intercomparison Project Phase 6 (CMIP6) experimental design and organization. *Geoscientific Model Development*, *9*(5), 1937–1958. https://doi.org/10.5194/gmd-9-1937-2016

Feyen, L., & Dankers, R. (2009). Impact of global warming on streamflow drought in Europe. *Journal of Geophysical Research*, *114*(D17), D17116. https://doi.org/10.1029/2008JD011438

Fleig, A. K., Tallaksen, L. M., Hisdal, H., & Demuth, S. (2006). A global evaluation of streamflow drought characteristics. *Hydrology and Earth System Sciences*, *10*(4), 535–552. https://doi.org/10.5194/hess-10-535-2006

Gan, R., Luo, Y., Zuo, Q., & Sun, L. (2015). Effects of projected climate change on the glacier and runoff generation in the Naryn River Basin, Central Asia. *Journal of Hydrology*, *523*, 240–251. https://doi.org/10.1016/j.jhydrol.2015.01.057

Gao, H. L., Tang, Q. H., Shi, X. G., Zhu, C. M., Bohn, T., Su, F. G., et al. (2010). Water budget record from variable infiltration capacity (VIC) model. In *Algorithm theoretical basis document for terrestrial water cycle data records* (pp. 120–173). Glasgow University.

Gelaro, R., McCarty, W., Suárez, M. J., Todling, R., Molod, A., Takacs, L., et al. (2017). The modern-era retrospective analysis for research and applications, version 2 (MERRA-2). *Journal of Climate*, *30*(14), 5419–5454. https://doi.org/10.1175/JCLI-D-16-0758.1

Hagg, W., Hoelzle, M., Wagner, S., Mayr, E., & Klose, Z. (2013). Glacier and runoff changes in the Rukhk catchment, upper Amu-Darya basin until 2050. *Global and Planetary Change*, *110*, 62–73. https://doi.org/10.1016/j.gloplacha.2013.05.005

Hall, J. W., Grey, D., Garrick, D., Fung, F., Brown, C., Dadson, S. J., & Sadoff, C. W. (2014). Coping with the curse of freshwater variability. *Science*, *346*(6208), 429–430. https://doi.org/10.1126/science.1257890

Heudorfer, B., & Stahl, K. (2017). Comparison of different threshold level methods for drought propagation analysis in Germany. *Hydrology Research*, *48*(5), 1311–1326. https://doi.org/10.2166/nh.2016.258

Hirabayashi, Y., Mahendran, R., Koirala, S., Konoshima, L., Yamazaki, D., Watanabe, S., et al. (2013). Global flood risk under climate change. *Nature Climate Change*, *3*(9), 816–821. https://doi.org/10.1038/nclimate1911

Hoang, L. P., Lauri, H., Kummu, M., Koponen, J., van Vliet, M. T. H., Supit, I., et al. (2016). Mekong River flow and hydrological extremes under climate change. *Hydrology and Earth System Sciences*, *20*(7), 3027–3041. https://doi.org/10.5194/hess-20-3027-2016

Hock, R. (2003). Temperature index melt modelling in mountain areas. *Journal of Hydrology*, *282*(1–4), 104–115. https://doi.org/10.1016/S0022-1694(03)00257-9

Hock, R., & Holmgren, B. (2005). A distributed surface energy-balance model for complex topography and its application. *Journal of Glaciology*, *51*(172), 25–36. https://doi.org/10.3189/172756505781829566

Horton, P., Schaefli, B., Mezghani, A., Hingray, B., & Musy, A. (2006). Assessment of climate-change impacts on alpine discharge regimes with climate model uncertainty. *Hydrological Processes*, *20*(10), 2091–2109. https://doi.org/10.1002/hyp.6197

Hosking, J. R. M. (1990). L-Moments: Analysis and estimation of distributions using linear combinations of order statistics. *Journal of the Royal Statistical Society: Series B*, *52*(1), 105–124. https://doi.org/10.1111/j.2517-6161.1990.tb01775.x

Huang, J., Su, F., Yao, T., & Sun, H. (2022). Runoff regime, change, and attribution in the upper Syr Darya and Amu Darya, central Asia. *Journal of Hydrometeorology*, *1*. https://doi.org/10.1175/JHM-D-22-0036.1

Huss, M., & Hock, R. (2018). Global-scale hydrological response to future glacier mass loss. *Nature Climate Change*, *8*(2), 135–140. https://doi.org/10.1038/s41558-017-0049-x

Immerzeel, W. W., & Bierkens, M. F. P. (2012). Asia's water balance. *Nature Geoscience*, *5*(12), 841–842. https://doi.org/10.1038/ngeo1643

Immerzeel, W. W., Lutz, A. F., Andrade, M., Bahl, A., Biemans, H., Bolch, T., et al. (2020). Importance and vulnerability of the world's water towers. *Nature*, *577*(7790), 364–369. https://doi.org/10.1038/s41586-019-1822-y

Immerzeel, W. W., van Beek, L. P. H., & Bierkens, M. F. P. (2010). Climate change will affect the Asian water towers. *Science*, *328*(5984), 1382–1385. https://doi.org/10.1126/science.1183188

Immerzeel, W. W., Wanders, N., Lutz, A. F., Shea, J. M., & Bierkens, M. F. P. (2015). Reconciling high-altitude precipitation in the upper Indus basin with glacier mass balances and runoff. *Hydrology and Earth System Sciences*, *19*(11), 4673–4687. https://doi.org/10.5194/hess-19-4673-2015

IPCC. (2014). *Climate change 2014: Synthesis report. Contribution of working groups I, II and III to the fifth assessment report of the intergovernmental panel on climate change*. IPCC.

Kan, B. Y., Su, F. G., Xu, B. Q., Xie, Y., Li, J. L., & Zhang, H. B. (2018). Generation of high mountain precipitation and temperature data for a quantitative assessment of flow regime in the upper Yarkant basin in the Karakoram. *Journal of Geophysical Research: Atmospheres*, *123*(16), 8462–8486. https://doi.org/10.1029/2017JD028055

Kaser, G., Großhauser, M., & Marzeion, B. (2010). Contribution potential of glaciers to water availability in different climate regimes. *Proceedings of the National Academy of Sciences*, *107*(47), 20223–20227. https://doi.org/10.1073/pnas.1008162107

Khanal, S., Lutz, A. F., Kraaijenbrink, P. D. A., van den Hurk, B., Yao, T. D., & Immerzeel, W. W. (2021). Variable 21st century climate change response for rivers in high mountain Asia at seasonal to decadal time scales. *Water Resources Research*, *57*(5), e2020WR029266. https://doi.org/10.1029/2020WR029266

Kraaijenbrink, P. D. A., Bierkens, M. F. P., Lutz, A. F., & Immerzeel, W. W. (2017). Impact of a global temperature rise of 1.5 degrees Celsius on Asia's glaciers. *Nature*, *549*(7671), 257–260. https://doi.org/10.1038/nature23878

Kraaijenbrink, P. D. A., Stigter, E. E., Yao, T. Y., & Immerzeel, W. W. (2021). Climate change decisive for Asia's snow meltwater supply. *Nature Climate Change*, *11*(7), 591–597. https://doi.org/10.1038/s41558-021-01074-x

Kumar, R., Singh, S., Kumar, R., Singh, A., Bhardwaj, A., Sam, L., et al. (2016). Development of a glacio-hydrological model for discharge and mass balance reconstruction. *Water Resources Management*, *30*(10), 3475–3492. https://doi.org/10.1007/s11269-016-1364-0

Li, C. H., Su, F. G., Yang, D. Q., Tong, K., Meng, F. C., & Kan, B. Y. (2018). Spatiotemporal variation of snow cover over the Tibetan Plateau based on MODIS snow product, 2001–2014. *International Journal of Climatology*, *38*(2), 708–728. https://doi.org/10.1002/joc.5204

Li, D., Yang, K., Tang, W., Li, X., Zhou, X., & Guo, D. (2020). Characterizing precipitation in high altitudes of the Western Tibetan plateau with a focus on major glacier areas. *International Journal of Climatology*, *1*(14), 5114–5127. https://doi.org/10.1002/joc.6509

Li, Y., Wang, C. H., & Su, F. G. (2021). Evaluation of climate in CMIP6 models over two third Pole subregions with contrasting circulation systems. *Journal of Climate*, *1*(aop), 1–64. https://doi.org/10.1175/JCLI-D-21-0214.1

Liang, X., Lettenmaier, D. P., Wood, E. F., & Burges, S. J. (1994). A simple hydrologically based model of land surface water and energy fluxes for general circulation models. *Journal of Geophysical Research*, *99*(D7), 14415–14428. https://doi.org/10.1029/94jd00483

Liang, X., Wood, E. F., & Lettenmaier, D. P. (1996). Surface soil moisture parameterization of the VIC-2L model: Evaluation and modification. *Global and Planetary Change*, *13*(1), 195–206. https://doi.org/10.1016/0921-8181(95)00046-1

Livneh, B., & Badger, A. M. (2020). Drought less predictable under declining future snowpack. *Nature Climate Change*, *10*(5), 452–458. https://doi.org/10.1038/s41558-020-0754-8

Lohmann, D., Raschke, E., Nijssen, B., & Lettenmaier, D. P. (1998). Regional scale hydrology: I. Formulation of the VIC-2L model coupled to a routing model. *Hydrological Sciences Journal*, *43*(1), 131–141. https://doi.org/10.1080/02626669809492107

Luo, Y., Wang, X., Piao, S. L., Sun, L., Ciais, P., Zhang, Y., et al. (2018). Contrasting streamflow regimes induced by melting glaciers across the Tien Shan–Pamir–North Karakoram. *Scientific Reports*, *8*(1), 1–9. https://doi.org/10.1038/s41598-018-34829-2

Lutz, A. F., Immerzeel, W. W., Kraaijenbrink, P. D. A., Shrestha, A. B., & Bierkens, M. F. P. (2016). Climate change impacts on the upper Indus hydrology: Sources, shifts and extremes. *PLoS One*, *11*(11), e0165630. https://doi.org/10.1371/journal.pone.0165630

Lutz, A. F., Immerzeel, W. W., Shrestha, A. B., & Bierkens, M. F. P. (2014). Consistent increase in High Asia's runoff due to increasing glacier melt and precipitation. *Nature Climate Change*, *4*(7), 587–592. https://doi.org/10.1038/nclimate2237

Maussion, F., Scherer, D., Mölg, T., Collier, E., Curio, J., & Finkelnburg, R. (2014). Precipitation seasonality and variability over the Tibetan plateau as resolved by the high Asia reanalysis. *Journal of Climate*, *27*(5), 1910–1927. https://doi.org/10.1175/JCLI-D-13-00282.1

Meng, F. C., Su, F. G., Li, Y., & Tong, K. (2019). Changes in terrestrial water storage during 2003–2014 and possible causes in Tibetan plateau. *Journal of Geophysical Research: Atmospheres*, *124*(6), 2909–2931. https://doi.org/10.1029/2018JD029552

Middelkoop, H., Daamen, K., Gellens, D., Grabs, W., Kwadijk, J. C. J., Lang, H., et al. (2001). Impact of climate change on hydrological regimes and water resources management in the Rhine Basin. *Climatic Change*, *49*(1), 105–128. https://doi.org/10.1023/A:1010784727448

Milner, A. M., Khamis, K., Battin, T. J., Brittain, J. E., Barrand, N. E., Füreder, L., et al. (2017). Glacier shrinkage driving global changes in downstream systems. *Proceedings of the National Academy of Sciences*, *114*(37), 9770–9778. https://doi.org/10.1073/pnas.1619807114

Mote, P. W., & Salathé, E. P. (2010). Future climate in the Pacific northwest. *Climatic Change*, *102*(1), 29–50. https://doi.org/10.1007/s10584-010-9848-z

Musselman, K. N., Lehner, F., Ikeda, K., Clark, M. P., Prein, A. F., Liu, C., et al. (2018). Projected increases and shifts in rain-on-snow flood risk over Western North America. *Nature Climate Change*, *8*(9), 808–812. https://doi.org/10.1038/s41558-018-0236-4

Nezlin, N. P., Kostianoy, A. G., & Lebedev, S. A. (2004). Interannual variations of the discharge of Amu Darya and Syr Darya estimated from global atmospheric precipitation. *Journal of Marine Systems*, *47*(1), 67–75. https://doi.org/10.1016/j.jmarsys.2003.12.009

Nuimura, T., Sakai, A., Taniguchi, K., Nagai, H., Lamsal, D., Tsutaki, S., et al. (2015). The GAMDAM Glacier Inventory: A quality-controlled inventory of Asian glaciers. *The Cryosphere*, *9*(3), 849–864. https://doi.org/10.5194/tc-9-849-2015

O'Neill, B. C., Tebaldi, C., van Vuuren, D. P., Eyring, V., Friedlingstein, P., Hurtt, G., et al. (2016). The scenario model intercomparison project (ScenarioMIP) for CMIP6. *Geoscientific Model Development*, *9*(9), 3461–3482. https://doi.org/10.5194/gmd-9-3461-2016

Palazzi, E., von Hardenberg, J., & Provenzale, A. (2013). Precipitation in the Hindu-Kush Karakoram Himalaya: Observations and future scenarios. *Journal of Geophysical Research: Atmospheres*, *118*(1), 85–100. https://doi.org/10.1029/2012JD018697

Pellicciotti, F., Buergi, C., Immerzeel, W. W., Konz, M., & Shrestha, A. B. (2012). Challenges and uncertainties in hydrological modeling of remote Hindu Kush–Karakoram–Himalayan (HKH) basins: Suggestions for calibration strategies. *Mountain Research and Development*, *32*(1), 39–50. https://doi.org/10.1659/MRD-JOURNAL-D-11-00092.1

Pritchard, H. D. (2019). Asia's shrinking glaciers protect large populations from drought stress. *Nature*, *569*(7758), 649–654. https://doi.org/10.1038/s41586-019-1240-1

Pritchard, H. D. (2021). Global data gaps in our knowledge of the terrestrial cryosphere. *Frontiers in Climate*, *3*, 51. https://doi.org/10.3389/fclim.2021.689823

Ragettli, S., Immerzeel, W. W., & Pellicciotti, F. (2016). Contrasting climate change impact on river flows from high-altitude catchments in the Himalayan and Andes Mountains. *Proceedings of the National Academy of Sciences*, *113*(33), 9222–9227. https://doi.org/10.1073/pnas.1606526113

Ragettli, S., Pellicciotti, F., Bordoy, R., & Immerzeel, W. W. (2013). Sources of uncertainty in modeling the glaciohydrological response of a Karakoram watershed to climate change. *Water Resources Research*, *49*(9), 6048–6066. https://doi.org/10.1002/wrcr.20450

Reichle, R., Liu, Q., Koster, R., Draper, C., Mahanama, S., & Partyka, T. (2017). Land surface precipitation in MERRA-2. *Journal of Climate*, *30*(5), 1643–1664. https://doi.org/10.1175/JCLI-D-16-0570.1

Ren, Z., Su, F., Xu, B., Xie, Y., & Kan, B. (2018). A coupled glacier-hydrology model and its application in eastern Pamir. *Journal of Geophysical Research: Atmospheres*, *123*(24), 13–692. https://doi.org/10.1029/2018JD028572

RGI Consortium. (2017). GLIMS: Global land ice measurements from space. *A Dataset of Global glacier outlines version 6.0 technical report*. https://doi.org/10.7265/N5-RGI-60

Rounce, D. R., Hock, R., & Shean, D. E. (2020). Glacier Mass change in high mountain Asia through 2100 using the open-source Python glacier evolution model (PyGEM). *Frontiers of Earth Science*, *7*, 331. https://doi.org/10.3389/feart.2019.00331

Rounce, D. R., Khurana, T., Short, M. B., Hock, R., Shean, D. E., & Brinkerhoff, D. J. (2020). Quantifying parameter uncertainty in a large-scale glacier evolution model using bayesian inference: Application to high mountain Asia. *Journal of Glaciology*, *66*(256), 175–187. https://doi.org/10.1017/jog.2019.91

Sakai, A. (2019). Brief communication: Updated GAMDAM glacier inventory over the high mountain Asia. *The Cryosphere*, *13*(7), 2043–2049. https://doi.org/10.5194/tc-13-2043-2019

Salathé, E. P., Jr. (2005). Downscaling simulations of future global climate with application to hydrologic modelling. *International Journal of Climatology*, *25*(4), 419–436. https://doi.org/10.1002/joc.1125

Salathe, E. P., Jr., Mote, P. W., & Wiley, M. W. (2007). Review of scenario selection and downscaling methods for the assessment of climate change impacts on hydrology in the United States Pacific Northwest. *International Journal of Climatology*, *27*(12), 1611–1621. https://doi.org/10.1002/joc.1540

Sarailidis, G., Vasiliades, L., & Loukas, A. (2019). Analysis of streamflow droughts using fixed and variable thresholds. *Hydrological Processes*, *33*(3), 414–431. https://doi.org/10.1002/hyp.13336

Sauer, I. J., Reese, R., Otto, C., Geiger, T., Willner, S. N., Guillod, B. P., et al. (2021). Climate signals in river flood damages emerge under sound regional disaggregation. *Nature Communications*, *12*(1), 2128. https://doi.org/10.1038/s41467-021-22153-9

Shea, J. M., Kraaijenbrink, P. D. A., Immerzeel, W. W., & Brun, F. (2021). Debris emergence elevations and glacier change. *Frontiers of Earth Science*, *9*, 709957. https://doi.org/10.3389/feart.2021.709957

Sheffield, J., Goteti, G. & Wood, E. F. (2006). Development of a 50-Year High-Resolution Global Dataset of Meteorological Forcings for Land Surface Modeling. *Journal of Climate*, *19*, 3088–3111. https://doi.org/10.1175/JCLI3790.1

Shrestha, R. R., Peters, D. L., & Schnorbus, M. A. (2014). Evaluating the ability of a hydrologic model to replicate hydro-ecologically relevant indicators. *Hydrological Processes*, *28*(14), 4294–4310. https://doi.org/10.1002/hyp.9997

Shrestha, R. R., Schnorbus, M. A., & Cannon, A. J. (2015). A dynamical climate model–driven hydrologic prediction system for the Fraser River, Canada. *Journal of Hydrometeorology*, *16*(3), 1273–1292. https://doi.org/10.1175/JHM-D-14-0167.1

Shukla, T., & Sen, I. S. (2021). Preparing for floods on the third Pole. *Science*, *372*(6539), 232–234. https://doi.org/10.1126/science.abh3558

Siegfried, T., Bernauer, T., Guiennet, R., Sellars, S., Robertson, A. W., Mankin, J., et al. (2011). Will climate change exacerbate water stress in Central Asia? *Climatic Change*, *112*(3–4), 881–899. https://doi.org/10.1007/s10584-011-0253-z

Singh, P., Kumar, N., & Arora, M. (2000). Degree-day factors for snow and ice for Dokriani Glacier, Garhwal Himalayas. *Journal of Hydrology*, *235*(1–2), 1–11. https://doi.org/10.1016/S0022-1694(00)00249-3

Sorg, A., Mosello, B., Shalpykova, G., Allan, A., Clarvis, M. H., & Stoffel, M. (2014). Coping with changing water resources: The case of the Syr Darya river basin in central Asia. *Environmental Science & Policy*, *43*, 68–77. https://doi.org/10.1016/j.envsci.2013.11.003

Stouffer, R. J., Eyring, V., Meehl, G. A., Bony, S., Senior, C., Stevens, B., & Taylor, K. E. (2017). CMIP5 scientific gaps and recommendations for CMIP6. *Bulletin of the American Meteorological Society*, *98*(1), 95–105. https://doi.org/10.1175/BAMS-D-15-00013.1

Su, F. G., Duan, X. L., Chen, D. L., Hao, Z. C., & Cuo, L. (2013). Evaluation of the global climate models in the CMIP5 over the Tibetan Plateau. *Journal of Climate*, *26*(10), 3187–3208. https://doi.org/10.1175/jcli-d-12-00321.1

Su, F. G., Zhang, L. L., Ou, T. H., Chen, D. L., Yao, T. D., Tong, K., & Qi, Y. (2016). Hydrological response to future climate changes for the major upstream river basins in the Tibetan plateau. *Global and Planetary Change*, *136*, 82–95. https://doi.org/10.1016/j.gloplacha.2015.10.012

Sun, H., & Su, F. (2020). Precipitation correction and reconstruction for streamflow simulation based on 262 rain gauges in the upper Brahmaputra of southern Tibetan Plateau. *Journal of Hydrology*, *590*, 125484. https://doi.org/10.1016/j.jhydrol.2020.125484

Sun, H., Su, F., Yao, T., He, Z., Tang, G., Huang, J., et al. (2021). General overestimation of ERA5 precipitation in flow simulations for High Mountain Asia basins. *Environmental Research Communications*, *3*(12), 121003. https://doi.org/10.1088/2515-7620/ac40f0

Sun, H., Su, F. G., He, Z., Ou, T., Chen, D. L., Li, Z. H., & Li, Y. (2021). Hydrological evaluation of high-resolution precipitation estimates from the WRF model in the Third Pole river basins. *Journal of Hydrometeorology*, *22*(8), 2055–2071. https://doi.org/10.1175/jhm-d-20-0272.1

Tong, K., Su, F. G., & Xu, B. Q. (2016). Quantifying the contribution of glacier meltwater in the expansion of the largest lake in Tibet. *Journal of Geophysical Research: Atmospheres*, *121*(19), 11158–11173. https://doi.org/10.1002/2016JD025424

Tong, K., Su, F. G., Yang, D. Q., Zhang, L. L., & Hao, Z. C. (2014). Tibetan plateau precipitation as depicted by gauge observations, reanalyses and satellite retrievals. *International Journal of Climatology*, *4*(34), 265–285. https://doi.org/10.1002/joc.3682

Unger-Shayesteh, K., Vorogushyn, S., Farinotti, D., Gafurov, A., Duethmann, D., Mandychev, A., & Merz, B. (2013). What do we know about past changes in the water cycle of central Asian headwaters? A review. *Global and Planetary Change*, *110*, 4–25. https://doi.org/10.1016/j.gloplacha.2013.02.004

United Nations (2019). Department of economic and social affairs. *Population Division*. https://population.un.org/wpp/

Varis, O., & Kummu, M. (2012). The major central Asian river basins: An assessment of vulnerability. *International Journal of Water Resources Development*, *28*(3), 433–452. https://doi.org/10.1080/07900627.2012.684309

Vogel, R. M., & Wilson, I. (1996). Probability distribution of annual maximum, mean, and minimum streamflows in the United States. *Journal of Hydrologic Engineering*, *1*(2), 69–76. https://doi.org/10.1061/(asce)1084-0699(1996)1:2(69)

Voosen, P. (2019). New climate models forecast a warming surge. *Science*, *364*(6437), 222–223. https://doi.org/10.1126/science.364.6437.222

Wang, X., Carrapa, B., Sun, Y. C., Dettman, D. L., Chapman, J. B., Caves Rugenstein, J. K., et al. (2020). The role of the westerlies and orography in Asian hydroclimate since the late Oligocene. *Geology*, *48*(7), 728–732. https://doi.org/10.1130/G47400.1

Werner, A. T. (2011). *BCSD downscaled transient climate projections for eight select GCMs over British Columbia. Victoria, BC: Pacific climate impacts Consortium* (p. 63). University of Victoria.

Wijngaard, R. R., Lutz, A. F., Nepal, S., Khanal, S., Pradhananga, S., Shrestha, A. B., & Immerzeel, W. W. (2017). Future changes in hydro-climatic extremes in the upper Indus, Ganges, and Brahmaputra river basins. *PLoS One*, *12*(12), e0190224. https://doi.org/10.1371/journal.pone.0190224

Wood, A. W., Leung, L. R., Sridhar, V., & Lettenmaier, D. P. (2004). Hydrologic implications of dynamical and statistical approaches to downscaling climate model outputs. *Climatic Change*, *62*(1), 189–216. https://doi.org/10.1023/B:CLIM.0000013685.99609.9e

Wood, A. W., Maurer, E. P., Kumar, A., & Lettenmaier, D. P. (2002). Long-range experimental hydrologic forecasting for the eastern United States. *Journal of Geophysical Research*, *107*(D20), 4429. https://doi.org/10.1029/2001JD000659

Wortmann, M., Bolch, T., Menz, C., Tong, J., & Krysanova, V. (2018). Comparison and correction of high-mountain precipitation data based on glacio-hydrological modeling in the Tarim river headwaters (high Asia). *Journal of Hydrometeorology*, *19*(5), 777–801. https://doi.org/10.1175/JHM-D-17-0106.1

Wortmann, M., Duethmann, D., Menz, C., Bolch, T., Huang, S., Tong, J., et al. (2022). Projected climate change and its impacts on glaciers and water resources in the headwaters of the Tarim River, NW China/Kyrgyzstan. *Climatic Change*, *171*(30), 1–24. https://doi.org/10.1007/s10584-022-03343-w

Yao, T. D., Thompson, L., Yang, W., Yu, W. S., Gao, Y., Guo, X. J., et al. (2012). Different glacier status with atmospheric circulations in Tibetan Plateau and surroundings. *Nature Climate Change*, *2*(9), 663–667. https://doi.org/10.1038/nclimate1580

Zhang, L. L., Su, F. G., Yang, D. Q., Hao, Z. C., & Tong, K. (2013). Discharge regime and simulation for the upstream of major rivers over Tibetan Plateau. *Journal of Geophysical Research: Atmospheres*, *118*(15), 8500–8518. https://doi.org/10.1002/jgrd.50665

Zhao, Q., Ding, Y., Wang, J., Gao, H., Zhang, S., Zhao, C., et al. (2019). Projecting climate change impacts on hydrological processes on the Tibetan Plateau with model calibration against the Glacier Inventory Data and observed streamflow. *Journal of Hydrology*, *573*, 60–81. https://doi.org/10.1016/j.jhydrol.2019.03.043

Zhao, Q., Zhang, S., Ding, Y. J., Wang, J., Han, H., Xu, J., et al. (2015). Modeling hydrologic response to climate change and shrinking glaciers in the highly glacierized kunma like river catchment, central tian Shan. *Journal of Hydrometeorology*, *16*(6), 2383–2402. https://doi.org/10.1175/jhm-d-14-0231.1

References From the Supporting Information

Arora, V. K., Scinocca, J. F., Boer, G. J., Christian, J. R., Denman, K. L., Flato, G. M., et al. (2011). Carbon emission limits required to satisfy future representative concentration pathways of greenhouse gases. *Geophysical Research Letters*, *38*(5), L05805. https://doi.org/10.1029/2010GL046270

Bentsen, M., Bethke, I., Debernard, J. B., Iversen, T., Kirkevåg, A., Seland, Ø., et al. (2013). The Norwegian Earth System Model, NorESM1-M – Part 1: Description and basic evaluation of the physical climate. *Geoscientific Model Development*, *6*(3), 687–720. https://doi.org/10.5194/gmd-6-687-2013

Bi, D., Dix, M., Marsland, S. J., O'Farrell, S., Rashid, H., Uotila, P., et al. (2013). The ACCESS coupled model: Description, control climate and evaluation. *Australian Meteorological and Oceanographic Journal*, *63*(1), 41–64. https://doi.org/10.22499/2.6301.004

Bolch, T., Pieczonka, T., Mukherjee, K., & Shea, J. (2017). Brief communication: Glaciers in the Hunza catchment (Karakoram) have been nearly in balance since the 1970s. *The Cryosphere*, *11*(1), 531–539. https://doi.org/10.5194/tc-11-531-2017

Brun, F., Berthier, E., Wagnon, P., Kääb, A., & Treichler, D. (2017). A spatially resolved estimate of High Mountain Asia glacier mass balances from 2000 to 2016. *Nature Geoscience*, *10*(9), 668–673. https://doi.org/10.1038/ngeo2999

Collins, W. J., Bellouin, N., Doutriaux-Boucher, M., Gedney, N., Halloran, P., Hinton, T., et al. (2011). Development and evaluation of an Earth-System model – HadGEM2. *Geoscientific Model Development*, *4*(4), 1051–1075. https://doi.org/10.5194/gmd-4-1051-2011

Defries, R. S., Hansen, M. C., Townshend, J. R. G., Janetos, A. C., & Loveland, T. R. (2000). A new global 1-km dataset of percentage tree cover derived from remote sensing: Global Percentage Tree Cover from Remote Sensing. *Global Change Biology*, *6*(2), 247–254. https://doi.org/10.1046/j.1365-2486.2000.00296.x

Donner, L. J., Wyman, B. L., Hemler, R. S., Horowitz, L. W., Ming, Y., Zhao, M., et al. (2011). The dynamical core, physical parameterizations, and basic simulation characteristics of the atmospheric component AM3 of the GFDL global coupled model CM3. *Journal of Climate*, *24*(13), 3484–3519. https://doi.org/10.1175/2011jcli3955.1

Duethmann, D., Zimmer, J., Gafurov, A., Güntner, A., Kriegel, D., Merz, B., & Vorogushyn, S. (2013). Evaluation of areal precipitation estimates based on downscaled reanalysis and station data by hydrological modelling. *Hydrology and Earth System Sciences*, *17*(7), 2415–2434. https://doi.org/10.5194/hess-17-2415-2013

Dufresne, J.-L., Foujols, M.-A., Denvil, S., Caubel, A., Marti, O., Aumont, O., et al. (2013). Climate change projections using the IPSL-CM5 Earth system model: From CMIP3 to CMIP5. *Climate Dynamics*, *40*(9), 2123–2165. https://doi.org/10.1007/s00382-012-1636-1

Dunne, J. P., John, J. G., Adcroft, A. J., Griffies, S. M., Hallberg, R. W., Shevliakova, E., et al. (2012). GFDL's ESM2 global coupled climate–carbon Earth system models. Part I: Physical formulation and baseline simulation characteristics. *Journal of Climate*, *25*(19), 6646–6665. https://doi.org/10.1175/jcli-d-11-00560.1

Farhan, S. B., Zhang, Y. S., Ma, Y. Z., Guo, Y. H., & Ma, N. (2015). Hydrological regimes under the conjunction of westerly and monsoon climates: A case investigation in the Astore Basin, Northwestern Himalaya. *Climate Dynamics*, *44*(11), 3015–3032. https://doi.org/10.1007/s00382-014-2409-9

Henn, B., Clark, M. P., Kavetski, D., McGurk, B., Painter, T. H., & Lundquist, J. D. (2016). Combining snow, streamflow, and precipitation gauge observations to infer basin-mean precipitation. *Water Resources Research*, *52*(11), 8700–8723. https://doi.org/10.1002/2015wr018564

Hoelzle, M., Azisov, E., Barandun, M., Huss, M., Farinotti, D., Gafurov, A., et al. (2017). Re-establishing glacier monitoring in Kyrgyzstan and Uzbekistan, Central Asia. *Geoscientific Instrumentation, Methods and Data Systems*, *6*(2), 397–418. https://doi.org/10.5194/gi-6-397-2017

Kääb, A., Treichler, D., Nuth, C., & Berthier, E. (2015). Brief communication: Contending estimates of 2003–2008 glacier mass balance over the Pamir–Karakoram–Himalaya. *The Cryosphere*, *9*(2), 557–564. https://doi.org/10.5194/tc-9-557-2015

Ma, Y., Zhang, Y., Yang, D., & Farhan, S. B. (2015). Precipitation bias variability versus various gauges under different climatic conditions over the Third Pole Environment (TPE) region. *Internal Journal of Climatology*, *35*(7), 1201–1211. https://doi.org/10.1002/joc.4045

Miller, R. L., Schmidt, G. A., Nazarenko, L. S., Tausnev, N., Bauer, S. E., DelGenio, A. D., et al. (2014). CMIP5 historical simulations (1850–2012) with GISS ModelE2. *Journal of Advances in Modeling Earth Systems*, *6*(2), 441–478. https://doi.org/10.1002/2013ms000266

Minora, U., Bocchiola, D., D'Agata, C., Maragno, D., Mayer, C., Lambrecht, A., et al. (2013). 2001–2010 glacier changes in the central Karakoram national park: A contribution to evaluate the magnitude and rate of the "Karakoram anomaly". *The Cryosphere Discussions*, *7*(3), 2891–2941. https://doi.org/10.5194/tcd-7-2891-2013

Qureshi, M. A., Yi, C., Xu, X., & Li, Y. (2017). Glacier status during the period 1973–2014 in the Hunza Basin, Western Karakoram. *Quaternary International*, *444*, 125–136. https://doi.org/10.1016/j.quaint.2016.08.029

Rotstayn, L. D., Collier, M. A., Dix, M. R., Feng, Y., Gordon, H. B., O'Farrell, S. P., et al. (2010). Improved simulation of Australian climate and ENSO-related rainfall variability in a global climate model with an interactive aerosol treatment. *International Journal of Climatology*, *30*(7), 1067–1088. https://doi.org/10.1002/joc.1952

Scoccimarro, E., Gualdi, S., Bellucci, A., Sanna, A., Fogli, P. G., Manzini, E., et al. (2011). Effects of tropical cyclones on ocean heat transport in a high-resolution coupled general circulation model. *Journal of Climate*, *24*(16), 4368–4384. https://doi.org/10.1175/2011JCLI4104.1

Shean, D. E., Bhushan, S., Montesano, P., Rounce, D. R., Arendt, A., & Osmanoglu, B. (2020). A systematic, regional assessment of high mountain Asia glacier mass balance. *Frontiers of Earth Science*, *7*, 363. https://doi.org/10.3389/feart.2019.00363

Voldoire, A., Sanchez-Gomez, E., y Mélia, D. S., Decharme, B., Cassou, C., Sénési, S., et al. (2013). The CNRM-CM5. 1 global climate model: Description and basic evaluation. *Climate Dynamics*, *40*(9), 2091–2121. https://doi.org/10.1007/s00382-011-1259-y

Volodin, E. M., Dianskii, N. A., & Gusev, A. V. (2010). Simulating present-day climate with the INMCM4. 0 coupled model of the atmospheric and oceanic general circulations. *Izvestiya - Atmospheric and Oceanic Physics*, *46*(4), 414–431. https://doi.org/10.1134/s000143381004002x

Watanabe, M., Suzuki, T., O'ishi, R., Komuro, Y., Watanabe, S., Emori, S., et al. (2010). Improved climate simulation by MIROC5: Mean states, variability, and climate sensitivity. *Journal of Climate*, *23*(23), 6312–6335. https://doi.org/10.1175/2010jcli3679.1

Yukimoto, S., Adachi, Y., Hosaka, M., Sakami, T., Yoshimura, H., Hirabara, M., et al. (2012). A new global climate model of the meteorological research institute: MRI-CGCM3—Model description and basic performance. *Journal of the Meteorological Society of Japan. Series II*, *90*(0), 23–64. https://doi.org/10.2151/jmsj.2012-a02

Zanchettin, D., Rubino, A., Matei, D., Bothe, O., & Jungclaus, J. H. (2013). Multidecadal-to-centennial SST variability in the MPI-ESM simulation ensemble for the last millennium. *Climate Dynamics*, *40*(5–6), 1301–1318. https://doi.org/10.1007/s00382-012-1361-9

Zhang, Y., Liu, S. Y., & Ding, Y. J. (2006). Observed degree-day factors and their spatial variation on glaciers in Western China. *Annals of Glaciology*, *43*, 301–306. https://doi.org/10.3189/172756406781811952

Zhou, Y., Li, Z., & Li, J. (2017). Slight glacier mass loss in the Karakoram region during the 1970s to 2000 revealed by KH-9 images and SRTM DEM. *Journal of Glaciology*, *63*(238), 331–342. https://doi.org/10.1017/jog.2016.142

Zhu, M., Yao, T., Xie, Y., Xu, B., Yang, W., & Yang, S. (2020). Mass balance of Muji Glacier, Northeastern Pamir, and its controlling climate factors. *Journal of Hydrology*, *590*, 125447. https://doi.org/10.1016/j.jhydrol.2020.125447

Zhu, M., Yao, T., Yang, W., Xu, B., Wu, G., Wang, X., & Xie, Y. (2018). Reconstruction of the mass balance of Muztag Ata No. 15 glacier, Eastern Pamir, and its climatic drivers. *Journal of Glaciology*, *64*(244), 259–274. https://doi.org/10.1017/jog.2018.16